Autonomous Tractor-Trailer Stopping and Jackknifing Dynamics

James Nathan Quartuccio

Thesis submitted to the faculty of the Virginia Polytechnic Institute and State University in partial fulfillment of the requirements for the degree of

Master of Science
In
Mechanical Engineering

Alfred L. Wicks, Chair
Steve C. Southward
Alan T. Asbeck

February 20, 2018
Blacksburg, Virginia

Keywords: Autonomous Vehicle, Tractor-trailer, LiDAR, Camera, Radar, Sensors, Stopping Distance, MATLAB®

Autonomous Tractor-Trailer Stopping and Jackknifing Dynamics

James Nathan Quartuccio

Academic Abstract

With the advancement of self-driving vehicles, roadways and highways will soon be driven entirely with fully autonomous vehicles. The presence of autonomous vehicles create safer roads that will no longer be hindered by driver misjudgments or distractions. Autonomy is not limited to passenger vehicles but can and is being applied to tractor-trailers. With the advancement in sensor perception range and resolution, it is now possible to consider creating a fully autonomous tractor-trailer that can see and identify far enough down the road that will stop in time so as to not hit an object.

The focus of this thesis is to provide recommendations based upon a dynamics model created for a forward-looking perception sensor for a tractor-trailer so that the vehicle can see far enough forward in order to stop and/or avoid collision as necessary and also when jackknifing may occur. In order to determine what the best forward sensor and sensor package is, review of previous autonomous systems and their sensor packages was performed. Additionally, how sensor technologies work shall be presented. The sensor technologies included are LiDAR, cameras, and radar. After this review, a model is presented that calculates the stopping distance of a tractor-trailer given certain parameters and variables such as initial velocity, braking factors, and steering angle for example. After such analysis, a brief discussion of the differences and recommendation between drum and disc brakes for an autonomous tractor-trailer shall be presented.

Autonomous Tractor-Trailer Stopping and Jackknifing Dynamics

James Nathan Quartuccio

Public Abstract

With autonomy becoming a reality for passenger cars, developing an autonomous for tractor-trailers is the next step for driverless roads. Tractor-trailers are heavy, large, and have a pivot joint between the tractor and trailer that makes the movement between the two more complicated. The purpose of the research presented here is to determine the best forward "looking" perception sensor that will see far out enough for the vehicle to stop in time to avoid hitting an object.

In order to determine the best sensor, a review of previous sensors and autonomous vehicle sensors will be explored along with the various perception technology. Additionally, a simulation of a tractor-trailer stopping was created to determine the range necessary for a forward perception sensor and when jackknifing may occur. The best brake type for a tractor-trailer will be recommended as well. Finally, the best forward sensor and senor layout for an autonomous tractor-trailer is made based upon the simulation results for the stopping distance of a tractor-trailer. The work, however, is not fully complete. A discussion of the future work and validation of the sensors selected will give future research goals.

Acknowledgements

I first want to thank my amazing and supportive wife. Without you, Hannah, I would not be finishing this. You are the love of my life. Thank you for sticking with me through all of this. There have been countless nights and weekends where you sat by my side and encouraged me in my work. I never doubted your support.

Thank you to Dr. Wicks, Dr. Southward, and Dr. Asbeck for your guidance and wisdom. I greatly appreciate the input, feedback, and encouragement that allowed me to achieve this research.

I also want to thank my parents, John and Katherine. I do not know how many times I have called the both of you for insight into your own experiences and knowledge. Thank you for always being there and supporting me. I owe so much to the both of you for the time and support you both gave me in higher education.

Thank you also to Denver Walling. You have been a great friend to me. I appreciated all the times I brought my research frustrations to you and how you somehow made me laugh.

Finally, thanks be to God. My rock and my foundation. Ephesians 5:20-21.

Contents

List of Figures

List of Tables

Chapter 1:

Introduction

1.1: Motivation

During a study from 2005-2007 approximately 95% of the 2 million crashes studied were attributed to driver error. The study found that of the driver error accidents, 41% were attributed to distractions or inattention and 33% to judgement errors [1]. Not only do these accidents cause loss in property, they lead to driver and pedestrian fatalities. In 2016, the National Highway Traffic Safety Administration (NHTSA) recorded a tractor-trailer driver fatality count of 722, and a total fatality count of vehicle drivers (all types of vehicles) and non-occupants of 37,461. Both of these totals are up from 2015 by 8.6% and 5.6% for tractor-trailer drives and total fatalities, respectively [2]. Even though tractor-trailer producers may make their vehicles safer, fatalities caused by the vehicle will still increase due to driver distractions and an increasing demand of goods transported by tractor-trailers. The number of fatalities that involved "Large Trucks and Buses" in 2015 was 4,311 which is up 8% from the previous year [3], and the total miles being traveled by tractor-trailers is increasing. NHTSA found the total miles traveled by tractor-trailers in 2013 to be 168 million miles which is up almost 5 million miles compared to 2012 and 28 million compared to a decade before it in 2003 [4]. A degree of autonomy in vehicles including tractor-trailers may be a solution to the driver error seen on today's roads.

The motivation of the research is, therefore, to provide a dynamics model that will provide the end user with information on safe driving parameters and stopping ranges for an autonomous tractor-trailer. The parameters that will be considered in the dynamics model include road/tire coefficient of friction, tractor and trailer weight, trailer center of gravity (CG) location, and tractor steering angle. Given these variables, the model will determine if jackknifing will occur or if the vehicle can safely operate and come to a stop.

With the conditions of jackknifing or safe operation known, the end user can evaluate which sensor technology should be selected for a forward-looking perception system. Information on various technologies be provided in the Literature Review chapter and the discussion of individual units will be presented after the results are shown. The challenges of determining the stopping distance and sensor for an autonomous tractor-trailer is in the vast differences between every tractor-trailer type. The mission of this thesis is to provide the end user with a tool with which to assess how tractor-trailer parameters and road conditions affect operations and what sensor units may be best under said conditions.

1.2: Thesis Outline

This thesis is developed to explore the area of tractor-trailer dynamics, determine the stopping distance, and recommend sensors based upon range requirements. The following chapter outline shows the path taken with the development of a tractor-trailer model, sensor discussion, and recommendations.

1. Literature Review

   The purpose of conducting a literature review is to determine the feasibility of creating an autonomous tractor-trailer. While there are companies that are in the prototype phase, not much literature has been presented on autonomous tractor-trailers. The literature review shall, therefore, discuss three different topics: basic autonomous vehicle, Team Oshkosh's vehicle and comparison to tractor-trailers, and sensor technologies for perception.

   In discussing basic autonomous vehicle, a basic understanding of how to create an autonomous vehicle and its sensor layout will be determined.

   Team Oshkosh's vehicle, although not a tractor-trailer, can give key insights into larger vehicle sensor selections and sensor layout. Although the dynamics of the vehicle are not the same, parallels can be drawn between the two types of vehicles since the Terra Max vehicle is much larger than a standard passenger vehicle.

   Finally, a discussion of the perception sensors available for an autonomous tractor-trailer is presented. The three sensor technologies discussed are LiDAR, cameras, and radar. These three technologies have been shown to have the capabilities to determine objects at long ranges.

2. Model and Calculations

   The Model and Results section discusses the process taken to develop the MATLAB® model of the tractor-trailer. The process involved development of a free body diagram. After the free body diagram is shown, the calculations used to determine the stopping distance and jackknifing stability shall be shown. After, discussion of each individual force affecting the tractor-vehicle will briefly be discussed. In addition to the forces, the MATLAB® model is presented along with discussion of each of the calculations being conducted.

3. Results

   The results of the MATLAB® model are shown. The results are first tested against known testing of coasting and braking to determine the accuracy of the model. After the model has been validated, the results are presented along with a presentation on possible sensors that can be used for an autonomous tractor-trailer. During the discussion of the results, a comparison shall be made between disc and drum brakes to determine which brake type offers better stopping distance and/or jackknifing stability.

4. Conclusion

Finally, the conclusion of this research is made. The conclusion will harp on the importance of understanding the dynamics behind an autonomous tractor-trailer in order to fully spec out a forward perception sensor. The end user will have an understanding and capability of how to select a sensor and how to use the model for both range requirements and to determine stability.

Chapter 2: Literature Review

Determining the perception sensors requires thorough review of the current technologies and how these sensors work. Validation of these sensors is crucial if an autonomous vehicle is to be trusted. To begin, a basic layout and autonomous capabilities are presented through Wuhan University and Zhou's autonomous vehicles. These vehicles are small in comparison to a tractor-trailer, but basic principles of sensor technologies and capabilities can be carried over to a tractor-trailer.

2.1.1: Wuhan University Autonomous Vehicle

The first example is Wuhan University's autonomous vehicle. The university employed a layout of three lasers and three cameras in the front of the vehicle. Each of these cameras and lasers were angled or placed at different levels to acquire the most range and observe in any blind spots of the others [6]. Looking over the sensor layout, each or the cameras and laser sensors cover crucial areas that would otherwise be missed. The lasers are pointed downward at varying angles. The laser labeled 1 sees long range, the second sees at a medium range, and the third sees immediately in front of the vehicle. Similarly, the cameras have differing fields of focus the first camera looks directly forward, and the second and third observe the sides [6].

All three lasers are used for the road and curb detection. If there are any irregularities in the road, the vehicle must be able to either stop or avoid the obstacle. The group determines the road and curb by utilizing the SICK laser scans.

While the vehicle may be able to detect the road, however, it needs a means to detect the lanes to follow. The cameras are, therefore, placed on the vehicle and positioned in this fashion to observe the lanes. If the vehicle was only traveling in a straight line, only the center camera would be necessary. However, since the vehicle must travel through turns, the side cameras pick up the lane markings as the vehicle is performing a turn.

In addition to lane detection, the cameras were used to perform sign recognition. Wuhan's vehicle was able to identify signs based off of two parameters: color and shape. The group separated the signs into six shape categories, and within each of these categories several colors were listed as possibly being found within the shape. For example, a no U-turn sign and speed limit sign are rectangular in shape with red, white, and black colors. If the camera sees a rectangular sign with white and black, it can deduct that it is a speed limit sign. Further matching and classification can be performed to determine the speed indicated. The vehicle also uses template to match what was seen by the cameras to determine what the sign was indicating using a SURF matching method. These templates are accessed after the shape and color have been determined for faster processing [6].

Overall, the group had extremely accurate results in sign detection. Using the process above, the group accurately determined 92.7% of the signs it encountered (265 signs in total). A method similar to [6] is highly recommended for an autonomous tractor-trailer. Detecting, processing, and identification of road signs quickly is imperative for tractor-trailers. Therefore, with the shape, color, and templet matching such as this will enable an autonomous tractor-trailer

to adjust speed per road sign direction, determine road hazards, and determine lane endings even at high speeds.

2.1.1.1: Wuhan University Tractor-trailer Applications

Wuhan University's vehicle, although small and has different dynamics compared to a tractor-trailer, has basic principles of autonomy are still applicable. The sensors although only front facing, give the general principle needed. The tractor-trailer autonomous vehicle may need several forward facing sensors to cover the full area in front of it. Depending on the type and position of the sensor, the area closest to the vehicle may be a blind spot. Placing additional short-range sensors in these blind spots will give the vehicle a better understanding of its surroundings; especially in residential areas where people or cyclists for example could enter these spots closest to the vehicle and not be picked up by the long-range sensors.

Additionally, the usage of cameras and LiDAR is well shown with Wuhan University's vehicle. The autonomous tractor-trailer must perform similar actions of lane and sign detection and determine the location of the road and curb through the sensors selected.

There are, however, a few drawbacks with Wuhan University's vehicle. First, a tractor-trailer is much larger with different dynamics and will, therefore, need different sensors. Additionally, the area covered by Wuhan's vehicle is insufficient for a tractor-trailer. If a tractor-trailer only had forward facing sensor, major blind spots around and behind the vehicle would be present. While how the sensors shall be used will be the same, further research into the placement and location still needs to be determined.

2.1.2: LiDAR and Camera Object Avoidance

A final basic example of autonomous vehicles is given with Zhou's autonomous vehicle. Although this example is very rudimentary in layout, the example shows the capabilities of sensor fusion for object avoidance. This vehicle uses two different sensors for the data fusion: cameras and LiDAR. Additionally, the combination of LiDAR and cameras also enables enhanced path planning for an autonomous vehicle. It is one-step to be able to identify an object and its location. Object avoiding, however, must be the next step. As has already been discussed, ensuring that a vehicle can adequately stop in time is the highest importance. If the vehicle can safely maneuverer around an object, however, such a maneuver will be preferred. Moving around an object safely will enable the vehicle to continue its route and prevent further backups behind it. Zhou presents such an option in his discussion on LiDAR and camera fusion.

Zhou presents a unique fusion of combining the camera image to a LiDAR point cloud information. As has been discussed, utilizing LiDAR information can give depth and greater information about an object. In order to obtain this fusion, Zhou used a Velodyne HDL-64E S2 LiDAR and Basler digital camera.

By utilizing the information obtained from the LiDAR about the road coordinates and position, each of the pixels of the camera can be given specific coordinates through matrix calculations between the LiDAR road coordinates that would have to be otherwise determined by methods mentioned earlier for monocular or binocular distance calculations. The benefits of this combination are that the two means of obtaining visual information are now unified. Objects detected by the LiDAR or camera can now be overlapped with the other system. This combination

will enable the negatives of one system to be negated by the other and for the vehicle to make smarter path planning decisions. For example, as Zhou's vehicle enters a curving road with a pedestrian in the middle of the current lane of travel. The camera images provide images for lane detection. The scans shown by Zhou show the road plane, trees on the sides, and the pedestrian in the middle of the road. The bottom left image shows the combination of the two sources overlapped. The LiDAR objects detected are either shown in a green or red box. The green boxes indicate that the vehicle will not hit the object, and the red boxes indicate that on the current path the vehicle will hit the object. The images therefore, show the new path chosen to avoid all obstacles in the former path [7].

2.1.2.1: Sensor Fusion for Tractor-trailer Applications

With the combination of LiDAR and cameras, a robust and accurate vision system can be developed. LiDAR cannot recognize signs, but cameras can. Cameras have difficulty determining distances or can fail to detect an object, but LiDAR can. For an autonomous tractor-trailer, using a camera and LiDAR data fusion can provide significant advantages in path planning. In residential or city areas, objects can appear in the path planned frequently. Identifying these objects and an appropriate path forward is essential so the vehicle can keep moving.

As with Wuhan University's vehicle, Zhou's vehicle also has several drawbacks when applied to a tractor-trailer. The sensor layout while it may cover the full area around the vehicle, will not work for a tractor-trailer. Having a LiDAR so high up on a tractor-trailer will cause severe blind spots to be present. As mentioned, adding sensors along the tractor-trailer will be a better approach. The direction with this layout, however, provides some insight on how to do this. The LiDAR selected by Zhou provides a full 360^{o} view around the vehicle. Using the same sensor in various positions around the vehicle could provide the necessary area of coverage.

Using the literature review from Wuhan University and Zhou provides a basic understanding of making a vehicle autonomous. The questions remain of what is the required range of a vision sensor and what sensors can reach the required range? Exploring Team Oshkosh's large autonomous vehicle will provide key insights into making a large vehicle autonomous.

2.1.3: Team Oshkosh

Finally, while Wuhan and Zhou have developed working vehicles, the vehicles are small when compared to a tractor-trailer and do not provide a satisfactory sensor layout that will be needed for a tractor-trailer. During the DARPA Urban Challenge, Team Oshkosh developed an autonomous medium tactical vehicle replacement truck. Although this truck is not a Class 8 tractor-trailer, the team converted a medium tactical vehicle replacement truck into an autonomous vehicle. The vehicle is much larger than a passenger vehicle and will give a better understanding of how to set up sensors to cover the surroundings of a tractor-trailer. The team chose to use more than just one sensor for perception; they chose LiDAR and multiple types of cameras for different perception capabilities [8].

Team Oshkosh uses an eleven camera system. The trinocular system in the front of the vehicle enables the vehicle to look forward and identify objects and lanes 40 m out. With the trinocular system, a three dimensional view of the surroundings is obtained enabling the vehicle to determine objects that may be in its path. In conjunction with the trinocular system, the stereo system in the front of the vehicle assists in detecting lanes. The monocular systems enables the

vehicle to perform merging into other lanes. The system enables the vehicle to identify and track other vehicle speeds in order to safely perform a merging maneuver. Similarly, the rear stereo and monocular system assist the vehicle in identifying vehicles or obstacles from behind. Again while merging, the vehicle needs to be able to determine how quickly other vehicles are approaching or if they are there at all. The combination of the rear and front systems enables this maneuver for the Oshkosh team [8].

Finally, in addition to all the camera's identifying vehicles, obstacles, and lanes, the vehicle has a LiDAR system that overlays these images for further information. The LiDAR system is used as a means of verification of objects since it has a higher accuracy in object detection. Additionally with the fusion of the images and LiDAR point cloud information, failures in object detection in one system are captured by the other since no object observed by one will be discarded. Utilizing the LiDAR points also assists the vision system in determining what the object seen is. For example, the LiDAR may be able to see that there is a sign post. However, the vision system may have failed to notice the object. With the LiDAR's help, the camera's can then focus on the sign and determine what is being stated by the sign. Perhaps the greatest strength of having the additional three LiDARs, however, is that there are now virtually no blind spots on the vehicle

The LiDAR set up utilized three individual LiDARs to give a wide FOV of the surroundings of the vehicle. As mentioned, this coverage enables the vehicle to accurately detect, identify, and plan a path for the vehicle around objects and in a dedicated lane of travel. The LiDARs utilized by Team Oshkosh provided a range of 80m. Utilizing this same system, the LiDAR's alone could provide adequate vision for an autonomous tractor-trailer system. However a fusion between the LiDAR and cameras can assist the vehicle in determining where and what the objects are. This fusion produces a disparity map. Having the position points from the LiDAR over top of the camera images provides further information of distance and shape to the image. With both the image and distance information provided by the two systems, the vehicle can identify the appropriate path to take.

2.1.3.1: Team Oshkosh Tractor-trailer Applications

Team Oshkosh gives the best sensor layout setup for a tractor-trailer. Since the team's vehicle is so large, several LiDAR sensor were used to cover the entire area around the vehicle for object detection negate blind spots from usage of a single sensor. Additionally, the usage of cameras all around the vehicle allows the vehicle to perform lane, object, and sign detection/identification also around the entire vehicle. For a tractor-trailer a similar layout and sensor usage will be necessary. Using a similar layout for a tractor-trailer will establish a baseline for this thesis research of a sensor layout.

There are, however, stark differences between Oshkosh's vehicle and a tractor-trailer. The tractor-trailer will have a trailer that will become angled with the tractor during turns and may potentially require a further range from its sensors due to a larger stopping distance. The dynamics of the tractor-trailer, therefore, shall dictate how these sensors are laid out. These dynamics are dictated by the fifth wheel of the tractor-trailer. The fifth wheel is the attachment point where the trailer connects to the tractor. The trailer is free to rotate around this fifth wheel. The dynamics of a tractor-trailer are, therefore, very different from Team Oshkosh's vehicle. The work done here to determine the stopping distance of a tractor-trailer must, therefore, take into account the fifth wheel dynamics.

Before discussing the stopping distance and sensor layout, however, sensor technologies that have the required range will need to be determined. A discussion of the possible sensor technologies will give a basic understanding of what technologies will actually work for perception are now presented.

2.2: Sensor Technologies

Before the stopping distance is determined, the final literature review section will discuss the technologies capable of perception for an autonomous tractor-trailer. The perception system is essentially the "sight" of the vehicle. It allows the any autonomous vehicle (not just tractor-trailers) to see what is in around them especially in the direction that the vehicle is headed given the development of perception algorithms and software to properly interpret the information from the sensor. Not only is the purpose of the sensor and software to determine the path the vehicle should take, but also whether or not there are objects or obstacles in the vehicles path.

Path planning especially for an autonomous tractor-trailer is crucial. Since the vehicle is traveling at such high speeds. It needs to plan its path out appropriately so as not to accidentally leave the road. Fortunately, major highways where tractor-trailers travel do not have sudden turns and is visible over long distances. The vision system, therefore, as has been discussed must be able to extend is "sight" to that of the stopping distance of the vehicle if not beyond. This will enable the vehicle to appropriately stop if it encounters impassable road conditions or stop if it is unable to identify the road accurately.

Additionally, the vehicle needs to be able to detect obstacles or undesirable road conditions. If there is an obstacle in the middle of the road, it is imperative that the vehicle be able to "see" this object and either maneuver or come to a complete stop to avoid causing an accident. The vehicle also needs to be able to identify road conditions that could cause the vehicle to become unstable and uncontrollable. Such road conditions include wet roads, snow, ice, uneven pavement, or holes.

Finally, a vision system needs to identify other vehicles around the tractor-trailer. In addition to identifying the location additionally processing must be conducted to determine how the other vehicle is travelling. Is the other vehicle stopping? Is the other vehicle encroaching into the path of travel? Such questions must be answered in order for the autonomous vehicle to behave appropriately and avoid collisions with other vehicles. The following list are the essentials that an autonomous vehicle must be able to perfume in a vision system:

1. Object Identification
2. Vehicle Tracking
3. Lane/Sign Detection
4. Range of sight for safe stopping

This thesis will not delve into the details of the software behind perception but instead focus on how a few perception sensor technologies work and what information they provide to software so that the user can decide which forward-looking sensor will best suite the user's requirements.

2.2.1: LiDAR Sensors

LiDAR is a vision system that obtains 3D information of its surroundings using a laser or lasers. LiDAR emits light towards its surroundings, and when the light hits objects or the ground, it returns back to the sensor. The sensor knowing how the light was emitted relative from the sensor and the time it takes for the light to return back can obtain the XYZ coordinates of what the light bounced off. Additionally, the returned light has an intensity value with which it is returned. While this is occurring the sensor is typically sweeping the more light across the surroundings to gather up to a 360^{o} viewing angle of its environment (up to a certain height). This sweeping action creates layers of returned light. These layers can then be used to understand where obstacles are and an appropriate path forward for an autonomous vehicle. The sweeping can be conducted using a single laser or multiple lasers to gather data. The XYZ coordinates and intensity from light points returned, is referred to the point cloud. One such company, Velodyne, produces LiDAR whose software creates a pint cloud.

As shown in the point cloud collected from the Velodyne LiDAR, a myriad of information is collected. The road with which the vehicle is travelling is seen as smooth with curbs on the sides. Obstacles such as trees and other vehicles can be easily determined based upon height and discontinuity from the level road.

Using the point cloud, an autonomous vehicle can determine planes that surround the vehicle based upon consecutive points being similar. Using the similarity, an autonomous system can route the vehicle to follow a path that has the same plane throughout. If there is a discontinuity in the plane though the examination of the data points an object or hole can be determined. The autonomous system can then choose to route the vehicle around, straddle, or come to a complete stop based upon the size of the object. LiDAR is designed to detect objects using the XYZ coordinates. All that is required is software to determine what constitutes an object.

The means by which LiDAR gathers information can take on different forms. Velodyne, for example, uses numerous lasers while spinning to obtain a 360^{o} point cloud. While this is excellent for most applications and positions on a vehicle, placing such an instrument on a tractor-trailer will cause sever blind spots. If the LiDAR is placed toward the front of the vehicle, the trailer will subsystem the view from behind. Figure 2.1 shows the limits of utilizing only one LiDAR at the front of the vehicle for object detection on a tractor-trailer.

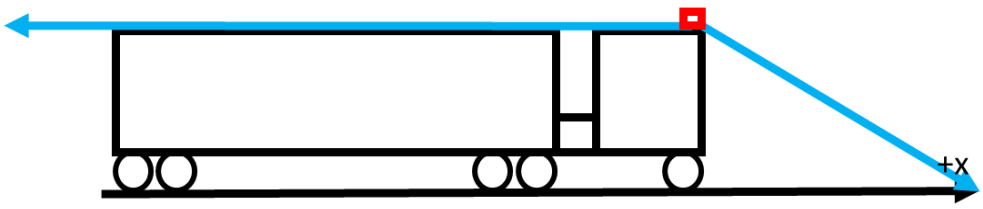

Figure 2.1: Single 360^{o} LiDAR viewing angle limits angles (sensor in red). Angles are not exact.

The use of a single Velodyne or any one LiDAR for object detection, therefore, is not recommended. For capturing all objects especially in autonomous reversing, an orientation such as shown in Figure 2.2 is much more suitable.

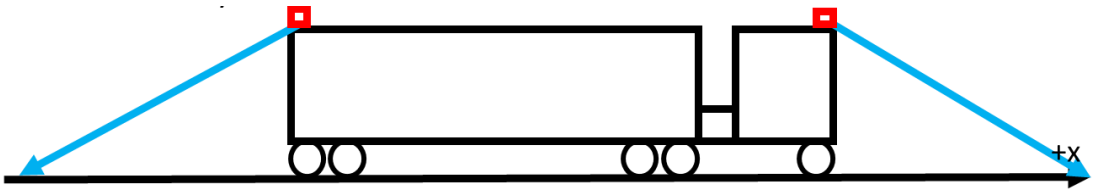

Figure 2.2: Two 360º LiDAR viewing angle limits (sensor in red). Angles are not exact.

Since the vehicle will not be traveling as quickly in reverse, a lesser ranged LiDAR or object sensor can be used. There are many LiDARs that can perform the necessary duties of object detection in the orientation shown in Figure 2.2. Velodyne and Sick are just a few LiDARs that can adequately perform object detection.

2.2.2: Camera Sensors

Having a vision system that relies on cameras can take on numerous different forms. A camera vision system can be a single, double, triple, or more cameras. Additionally, these cameras can be more specific in what they "see." There are many unique cameras that focus on specific light spectrums, resolutions, or intensities. The usage of these different cameras allows varying objects to be more easily identified or disregarded depending on the object. For example, live vegetation can easily be identified due to its specific color range of green. Road signs and lane markings can be identified based off of color, geometry of the object, or intensity with which the light reflects off of the object.

2.2.2.1: Monocular Optic

Monocular vision utilizes only a single camera to capture information. An example of a monocular camera system can be seen in the work done by Diamantas et al [10]. The group used the camera qualities discussed (resolution and focal length) in addition to the height that the camera is fixed at to determine how far away an object is.

In order to perform the distance calculation, however, the camera must first be calibrated to determine the camera height in pixels (H_{Cp}). Having the camera pixel height is the means by which the system can reference a known point. With the reference, any bounding box that is placed around the object (with the bottom showing) does not need to be fully accurate. In order to calibrate the system therefore, the height of the camera (H_{Cm}) and the height of the object in meters (H_{Om}) and pixels (H_{Op}) (from the camera's picture) must be known. Once these three parameters have been established, the Equation 1, acquired from [10], can be used to determine the camera height in pixels.

$$\frac{H_{Cm}}{H_{Cp}} = \frac{H_{Om}}{H_{Op}} \tag{1}$$

With the camera height in meters and pixels established, we can use the ratio in Equation 1 to determine the unknown object height. Additionally, the camera focal length (f_{mm}) and height (H_{Smm}) are also known. Therefore, after determining the size of the object in pixels and the overall image height (H_{Imgp}), the distance (d) can be found using Equation 2, acquired from [10].

$$d = \frac{f_{mm} H_{Om} H_{Imgp}}{H_{Op} H_{Smm}} \tag{2}$$

After the calibration and software have been set up, distance calculations for a detected object can thus be easily and rapidly determined. The group was highly effective at determining the height of objects with very little error. Table 2.1 shows the distance calculation results from a calibrated and uncalibrated camera compared to the actual distance.

Table 2.1: Diamantas et al. distance calculation results compared to the actual distance [10].

Trial	Actual Distance (m)	Calculated Distance (m) (calibrated/Uncalibrated)
1	7	6.99/7.34
2	14	14.08/14.78
3	21	20.75/21.77
4	28	27.16/28.5
5	5	5.12/5.38
6	10	10.39/10.19
7	13	13.77/14.46

The results obtained by the group are reliable. The mean relative error for distance calculations of a calibrated and uncalibrated camera are 2.44% and 6.25% respectively [10].

The benefits of using a single camera over two or more can be found in calibration. The user does not need to precisely measure the distance between cameras or worry about one vibrating differently relative to the other in order for software to have the accuracy required. A single camera is much cheaper compared to purchasing multiples. Additionally, mounting a single camera is simpler then precisely mounting two cameras next to each other. However, a single camera has many cons as well. While a lens may be added that adds a wider range in terms of seeing further out or a wider view, information can be lost in terms of angle of view or resolution, respectively.

2.2.2.2: Binocular Camera Sensors

Binocular vision as the name implies uses two cameras to obtain distance information. Similar to monocular vision, it is essential to know the focal length of the camera; however, the resolution of the cameras is not utilized in distance equation (although still no less important in determining an accurate measurement).

As with monocular vision, binocular vision takes a point of interest in an image to determine how far away an object is located. While there are multiple methods to determine what point to take, this research shall briefly discuss a method used by Ventroux et al. The group broke down the object detection into three separate steps. The first step is improving the images to remove any distortions. The second step is to apply a filter to remove any false matches between the images in the next step. Finally, a disparity map is applied to match up the point of interest [11]. If pixels are filtered for intensity, there is a range from 0-255 that a pixel can be. Therefore, if two identical images are aligned their pixels will match up accordingly (assuming that the images are the exactly same). In binocular vision, however, the images are slightly shifted and thus the

pixels are shifted in location. Ventroux et al. therefore, took a kernel that has the point of interest and sweeps it across the placed "search line" in the other image. When the kernel's pixels lined up with the pixel in the other image there was a match. This distance it took for there to be a match was the difference between two images' point of interest (*D*).

As with the monocular vision distance equation, the focal length (*f*) is again necessary to determine distance. Additionally, the distance (*B*) between the cameras is essential to know. Equation 3 from [11] shows the object distance (*P*) calculation for binocular vision.

$$P = \frac{B*f}{D} \tag{3}$$

The system developed proved to be much quicker than a humans ability and highly accurate. The group achieved a zero-error identification system with +/- 3 m at 40 m. Although the data of these results are not available, the system none the less is very reliable for a tractor-trailer system assuming the range can be further extended out.

This example again shows how important resolution and focal length are for binocular vision as with monocular vision or any vision system. If the cameras resolution is poor, it will be unable to determine key points of interest causing objects to go undetected because the algorithms will be unable to compare the images. If the images resolution is extremely good, however, there will be a greater lag in the image processing since it will have to sweep through more pixels. If the focal length is too far out, the system will not pick up object close by. If too close, further objects may not be seen. The balance between poor and excellent resolution or close and far focal length, therefore, must be determined by the user based on application.

While compared to monocular vision, binocular vison has many benefits. Instead of having one image for comparison, two images can be compared to each other to prevent any false detections. Additionally, distance calculations are not dependent on seeing the base of an object. If a portion of an object is detected, distance calculations can be made regardless of seeing the bottom. The height of the cameras also does not matter for calculations. This is essential since most vehicle will oscillate due to differing road conditions which can cause incorrect distances in a monocular system. If a camera happens to fail, the vehicle won't become blind, but it could use a single camera to perform stopping duties for example. Binocular vision is not without its downfalls, however. The added camera raises cost along with additional calibration. If the cameras position relative to each other is not properly calibrated, incorrect distances can be given.

2.2.3: Radar Sensors

The final sensor that shall be explored for its potential usage on an autonomous tractor-trailer is radar. Radar operates in a very similar fashion to LiDAR for detecting objects. Instead of using light however, radar uses radio waves. The radio wave is emitted from the sensor, and based off the return of the wave, an objects' location can be determined. The Doppler effect is how the radar determines information such as relative velocity and location from the returning wave [12]. However, radar has many better benefits over LiDAR. Radar typically has greater ranges than LiDAR and is typically cheaper. The greatest advantage Radar has over LiDAR, however, is its ability to maintain operability in inclement weather. While pulling off the road is an appropriate course of action, radar will give the vehicle the ability to still perceive through snow where cameras and LiDAR will fail, and can therefore still travel. Radar, however, for most models is not as

precise as LiDAR in its resolution; and as with LiDAR, radar cannot sense the same way a camera does. Therefore, radar cannot be used to determine signs or lane markings.

When a radar frequency (F_t) is emitted, it has a different frequency upon returning back to the sensor. The frequency is called the beat frequency (f_b). The time (t_d) is simply the time difference between the emitted wave and returned waves. In order to determine the range (R) at which the wave hit something, Equation 4 is used [13].

$$t_d = \frac{c*R}{2} \tag{4}$$

Where c is the speed of light ($3*10^8$ m/s). The velocity of the object is determined using Equation 5 [12].

$$f_b = F_t \frac{v \cos\theta \cos\emptyset}{c} \tag{5}$$

Where v is the velocity, θ is the horizontal angle between the emitted radar and the object, and ϕ is the elevation angle between the emitted radar and object.

From Equations 4 and 5, the user can determine the range based off of time and velocity from the returned frequency. Computing this information, however, still lacks a crucial element. The returned frequency needs to be filtered from the noise of the sensor. In order to determine the peaks in the frequency where the objects are, a Fast Fourier Transform (FFT) must be performed. The FFT takes the information in the time domain and converts it to the frequency domain. This allows the user to determine that two returned frequencies are above the noise floor. These frequencies indicate that objects are located at the given range and have the determined relative velocity. The location allows the vehicle to determine if the object is in the designated path of travel. With the relative velocity, the vehicles software can then decide if it is appropriate to stop or if it is safe to keep traveling if the object is another vehicle traveling with it.

2.3: Delays and Guidelines

While it is critical to take into account all the various forces acting on the vehicle, it is important to also consider any potential delays and constraints that the vehicle must operate under. Not only does the user need to consider the delay from when the brake pedal is compressed to when the brakes are applied at the wheel, but with an autonomous system, the processing time must also be considered. As with a human driver, recognition or processing time is required with an autonomous vehicle. Depending on the software involved and data sent from the sensor, the processing time can vary.

While the focus of this thesis is on distance requirements for a forward sensor instead of the processing software, it is still critical to take into account processing delays for said sensors. For cameras according to Lan and Zhang, the processing delay can be up to .039 s for some software [13]. According to Ren, the processing time of their software for cameras was higher at approximately .2 s to process each image [14]. For LiDAR sensors used by Chen et al, the delay was determined to be approximately 0.1 s to process obstacles [15]. For radar used by Ha et al, the processing time was approximately 0.46 s to process obstacle [16] For purposes of this thesis'

simulations, the delay in processing will be taken into consideration. For the simulations, a worst case will be considered by using a delay of 0.55 s.

In addition to taking into consideration delays due to processing, the user needs to consider federal guidelines for the tractor-trailer. According to the Department of Transportation National Highway Traffic Safety Administration, there are several guidelines that tractor-trailer air brakes must satisfy. According to the most recent FMVSS No. 121 guidelines:

> "For heavy trucks in the loaded-to-GVWR (Gross Vehicle Weight Rating) condition, the stopping distance requirements form an initial speed of 60mph are as follows. A tractor with two or three axles and a GVWR of 70,000 pounds or less must stop within 250 feet. A tractor with three axles and a GVWR greater than 70,000 pounds must stop within 310 feet. A tractor with four or more axles and a GVWR of 85,000 pounds or less must stop within 250 feet. A tractor with four or more axles and a GVWR greater than 85,000 must stop within 310 feet." [14]

For the purposes of this research, it is important to keep these guidelines and extrapolate whether it is acceptable to consider higher speeds at the same conditions. Even though a tractor-trailer may not jackknife and come to a stop but not meet the FMVSS stopping distance, the operating condition should not be considered. This stopping distance does not just include when the brakes are initially pressed, but should also include the processing time delay.

Chapter 3: Model and Calculations

The model created for this research is now presented. The model created here uses information from multiple sources on vehicle dynamics that will be referenced throughout. The purpose of creating this model, is to provide the end user with a region of operation that the vehicle can operate within. With the creation of this model, future research can also use it for vehicle path planning and controls which shall be discussed in Chapter 4.

3.1: Tractor-Trailer Model

In order to determine the required range for a perception sensor for a tractor-trailer, a MATLAB® model was created. The purpose of the model was to determine the stopping distances given multiple parameters, differing weight, and at various initial velocities. With these stopping distances, given initial velocity conditions, and tractor-trailer parameters, a perception sensor appropriate for an autonomous tractor-trailer can be recommended in addition to the maximum velocity that the vehicle can travel at while being able to stop safely and in an appropriate distance.

Over the following sections, the MATLAB® model development is presented. The first step, the Free Body Diagram (FBD), is discussed and the dimensions involved. Each force is then discussed and how it affects the model. Along with the forces, the parameters and variables are discussed in addition to the variables that are changed between simulations to gather a data set that will enable a sensor to be selected. Next, the velocity and position (distance traveled) are calculated using the acceleration from the force calculations. Finally, the development of the model code is then shown.

3.1.1: FBD of the Tractor-trailer

In order to properly model and simulate the tractor-trailer, a FBD was developed. For this model there are several different assumptions that are being used. The assumptions and simplifications are as follows:

1. The vehicle will be considered to be braking without anti-lock brakes.
2. No engine force is being added to accelerate or engine brake.
3. No slosh is occurring in the tractor or trailer (the tractor and trailer are considered rigid).
4. No rolling or pitching is occurring.
5. Axles 2 and 3 are combined together and positioned directly below the fifth wheel.
6. Axles 4 and 5 are combined together.

For this model, the vehicle is simulated to be deaccelerating until stopped. The main acting force on the system is the braking force which enables the vehicle to stop quickly. The remaining forces are the drag force, normal force, gravitational force, rolling resistance force, and cornering force. All of these forces will be discussed in more detail in the following sections after the system of equations to solve for the unknowns is developed.

Since the tractor-trailer will be traveling through a curve to study the jackknifing behavior, the model can not be treated as a single point mass. By creating a FBD of the tractor and trailer separately for turning, the model is separated into two point masses coupled at the fifth wheel. When the front wheels of the tractor are turned, the trailer will not stay laterally behind the tractor due to the pivot point, known as the fifth wheel, which connects the trailer to the tractor. The fifth wheel gives the tractor a rotational degree of freedom. The fifth wheel typically sits between the two rear axles of the tractor.

Figure 3.1 shows the top down view of the tractor-trailer executing a turn or traveling through a curve. The figure depicts only a single angle out of a multitude of possible angles. From the figure, the tractor and trailer will be separated into individual FBDs. The difference between the turning FBDs and the straight line FBDs are the separated masses, the angle between the tractor and trailer, the cornering force, and the separated x and y accelerations. In Figure 3.1, the tractor and trailer CG locations and axles are pointed out (these positions are not exact).

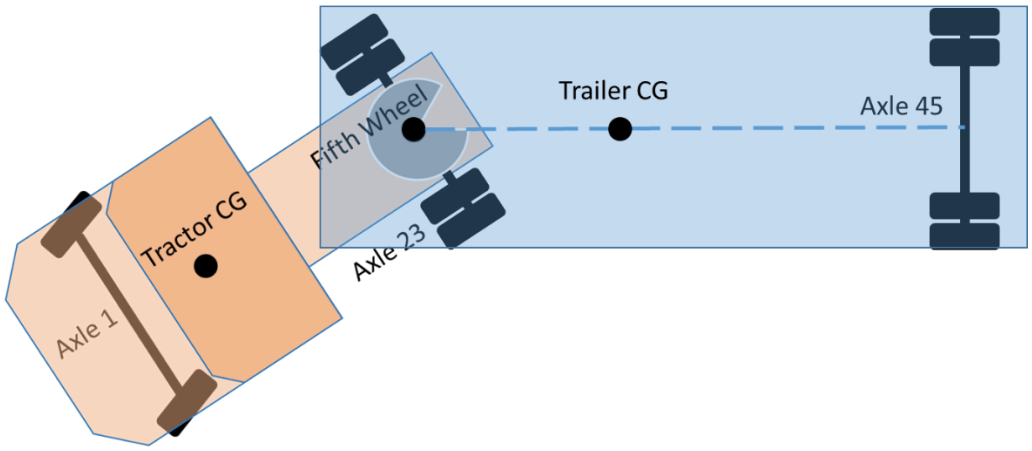

Figure 3.1: Turning tractor-trailer diagram from top down. The CG and axle positions are not exact.

Expanding from Figure 3.1, the tractor and trailer are now observed individually. Figure 3.2 and Figure 3.3 show the top down views of the tractor for the forces and dimensions in the x and y directions. Here the additional forces for cornering and the hitch forces are shown. The hitch forces are a result of separating the tractor and trailer and represent the coupling between the two. Additionally, the tractor and trailer have separate coordinate system when the FBDs are separated.

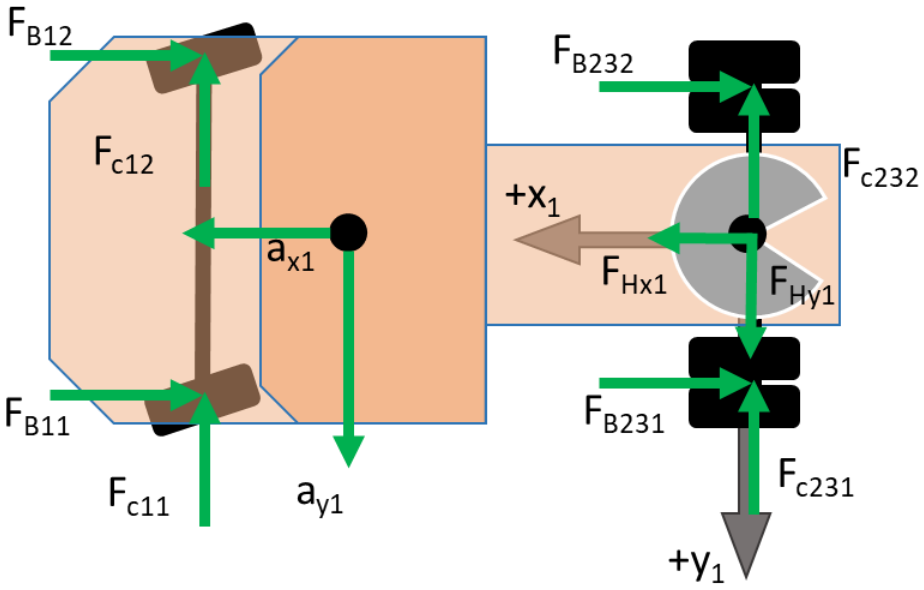

Figure 3.2: Top down view of the tractor showing the forces acting on the vehicle in the x and z directions

In Figure 3.2, the cornering forces are as follows, F_{c11} is the cornering force for the front left wheel, F_{c12} is the cornering force for the front right wheel, F_{c231} is the cornering force for the back left wheel, and F_{c232} is the cornering force for the back right wheel. For the braking forces, F_{B11} is the braking force for the front left wheel, F_{B12} is the braking force for the front right wheel, F_{B21} is the braking force for the back left wheel, and F_{B22} is the braking force for the back right wheel. The final variables are the accelerations in the x (a_{x1}) and y (a_{y1}) and the hitch forces in the x (F_{Hx}) and y (F_{Hy}).

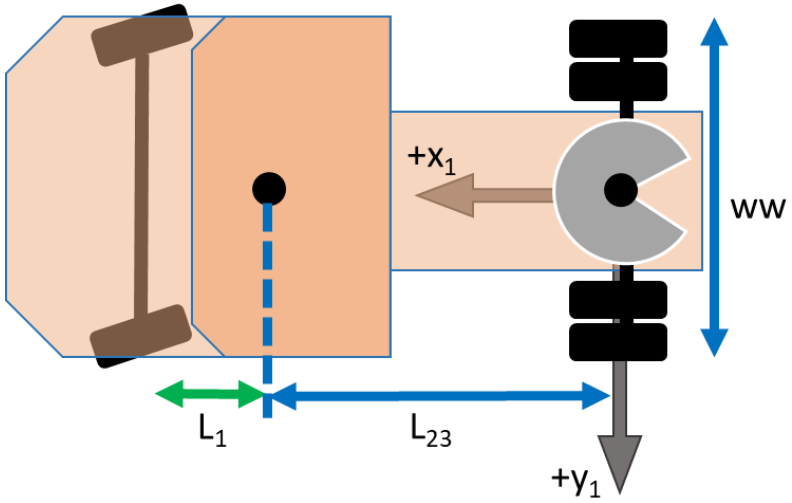

Figure 3.3: Top down view of the tractor showing the dimensions of the vehicle.

In Figure 3.3, the variables are the lengths from the front axle to the tractor CG (L_1), from the rear axle to the tractor CG (L_{23}), and the width from wheel to wheel (ww).

Figure 3.4 and Figure 3.5 show the side views of the tractor for the forces and dimensions in the x and z directions. The final hitch force in the z direction can now be seen.

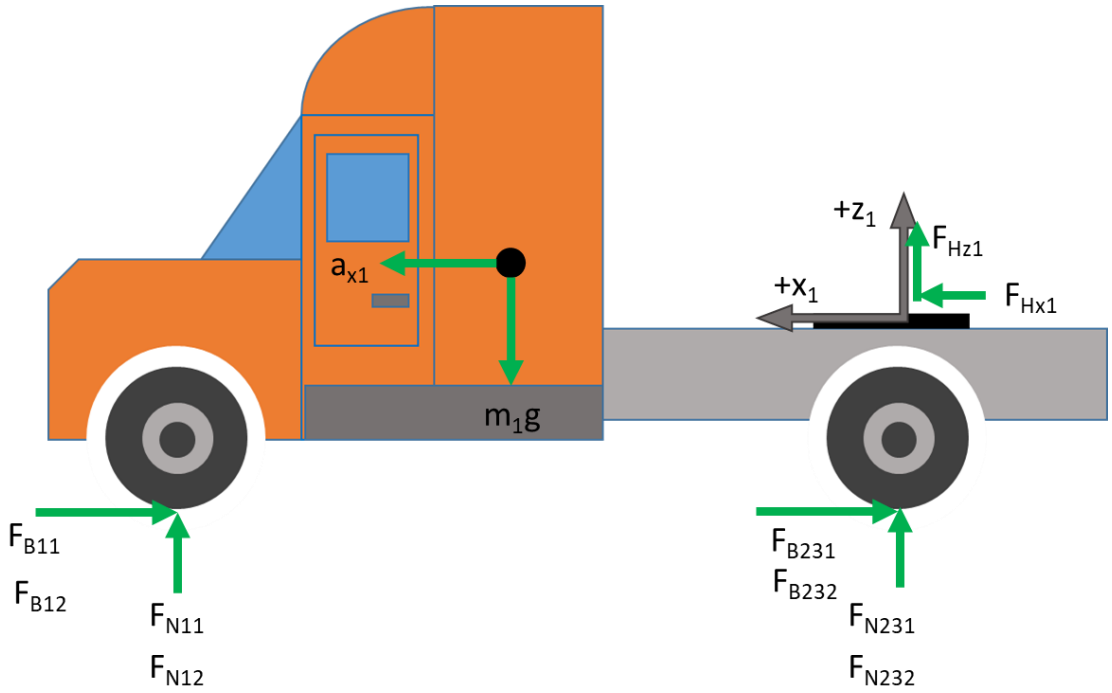

Figure 3.4: Side view of the tractor showing the forces acting on the vehicle in the x and z directions

In Figure 3.4, the normal forces, hitch force in the z-direction, and gravitational pull are now shown in addition to several of the other forces already mentioned. The hitch force is labeled as F_{Hz}. The normal forces F_{N11} and F_{N12} are applied at the front left and right respectively. The normal forces are F_{N231} and F_{N232} are applied at the back left and right, respectively. In order to simplify the calculations for moments, cornering force, rolling resistance, or braking later, the normal forces are combined using Equations 6 through 9.

$$F_{NR} = F_{N12} + F_{N232} \quad (6)$$

$$F_{NL} = F_{N11} + F_{N231} \quad (7)$$

$$F_{N1} = F_{N11} + F_{N12} \quad (8)$$

$$F_{N23} = F_{N231} + F_{N232} \quad (9)$$

In addition to a side view of the forces, Figure 3.5 is shown below to capture the dimensions from a side view not shown in a top down view.

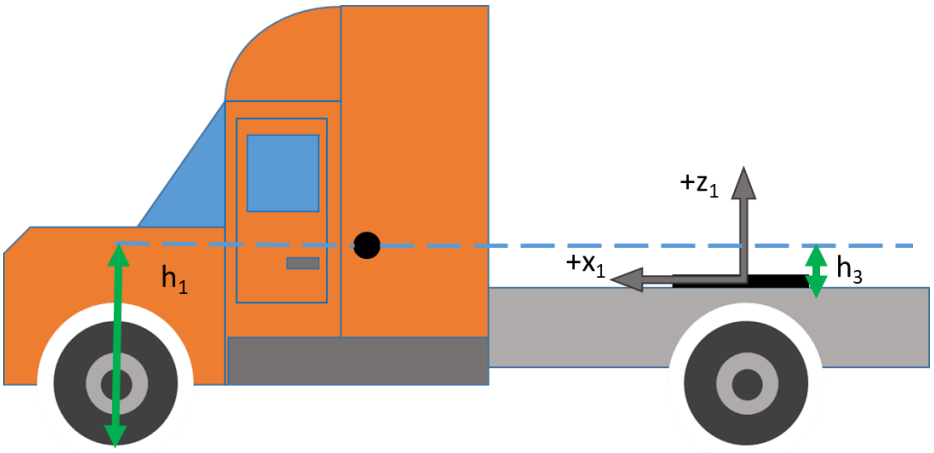

Figure 3.5: Side view of the tractor showing the dimensions of the vehicle.

In Figure 3.5, the constants h_1 and h_3 are the distances from the bottom of the wheel to the tractor CG and the height from the fifth wheel to the tractor CG.

As with the tractor, the FBDs and dimensions for the trailer shall now be shown. Figure 3.6 and Figure 3.7 show the top down view of the tractor for the forces and dimensions in the x and y directions. The hitch forces are the same forces as shown acting on the tractor, but here the forces are in the opposite direction as to Newton's Third Law. Additionally, the hitch forces will have a varied angle as the trailer changes its angle relative to the tractor. These calculations will be shown later.

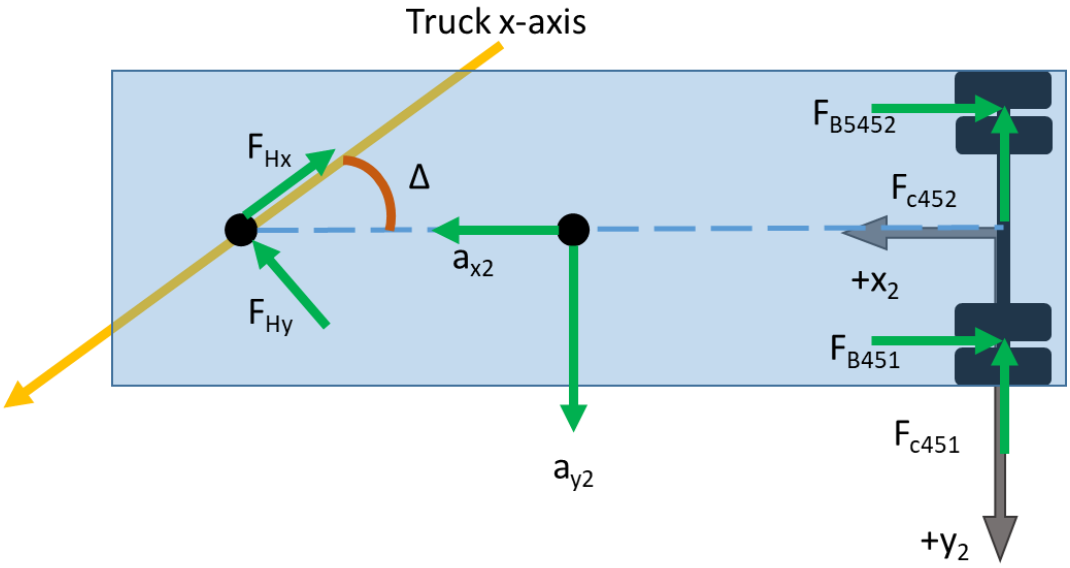

Figure 3.6: Top down view of the trailer showing the forces acting on the vehicle in the x and z directions

In Figure 3.6, the cornering forces are as follows, F_{c451} is the cornering force for the left wheel and F_{c452} is the cornering force for the right wheel. For the braking forces, F_{B451} is the braking force for the front left wheel and F_{B452} is the braking force for the right wheel. The other variables are

the accelerations in the x (a_{x2}) and y (a_{y2}), the hitch forces in the x (F_{Hx}) and y (F_{Hy}), and the trailer angle Δ.

$$\Delta = \tan^{-1}\left(\frac{L_6 - L_2}{r_2}\right) + \sin^{-1}\left(\frac{L_7 + L_4}{\sqrt{(L_6 - L_2)^2 + r_2{}^2}}\right) \quad (10)$$

$$r_2 = \frac{L_2 + L_1}{\tan(\Delta)} + ww \quad (11)$$

As with Figure 3.6 showing the forces from a top down perspective, Figure 3.7 shows the top down view with the dimensions.

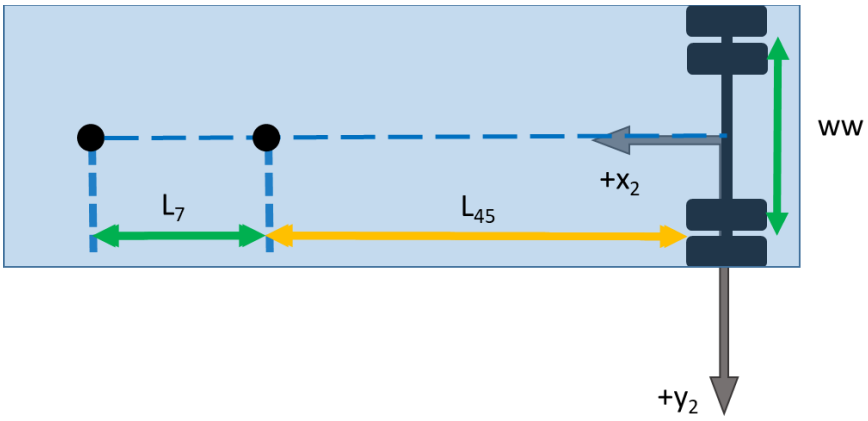

Figure 3.7: Top down view of the trailer showing the dimensions of the vehicle.

The dimension L_7 and L_{45} are the changing dimensions to simulate a new CG position in different runs. The purpose of changing these dimensions is not only to observe the effect the CG location will have on the stopping distance but also the stability of the trailer (in terms of yaw). The effect is due to the CG location affecting the normal forces which in turn affect various other forces.

Figure 3.8 and Figure 3.9 show the side view of the trailer to shown the forces and dimensions in the x and z directions.

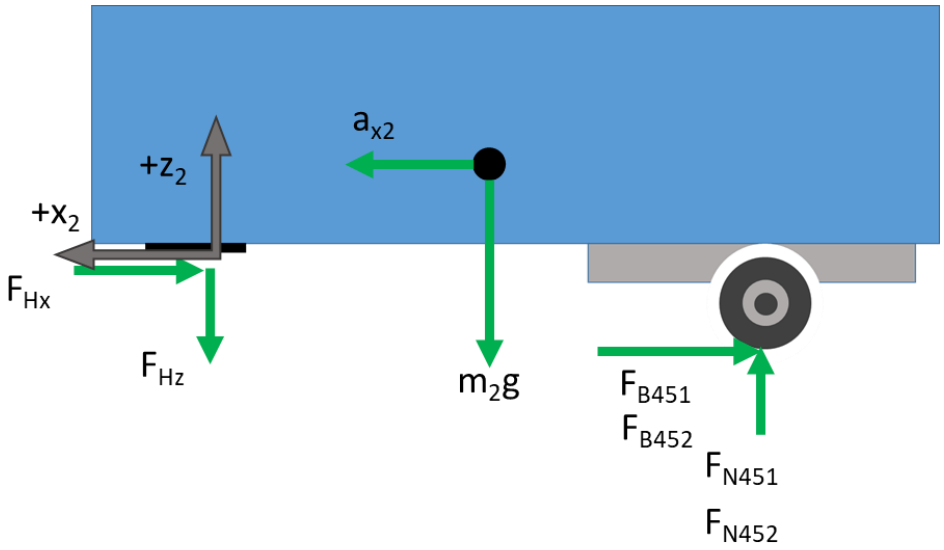

Figure 3.8: Side view of the trailer showing the forces acting on the vehicle in the x and z directions

As with the tractor side view, Figure 3.8 shows the normal forces, hitch force in the z-direction, and gravitational pull in addition to several of the other forces already mentioned. The hitch force is labeled as F_{Hz}. The normal forces F_{N451} and F_{N452} are applied at the left and right respectively. In addition to the forces, Figure 3.9 shows the height parameters for the trailer.

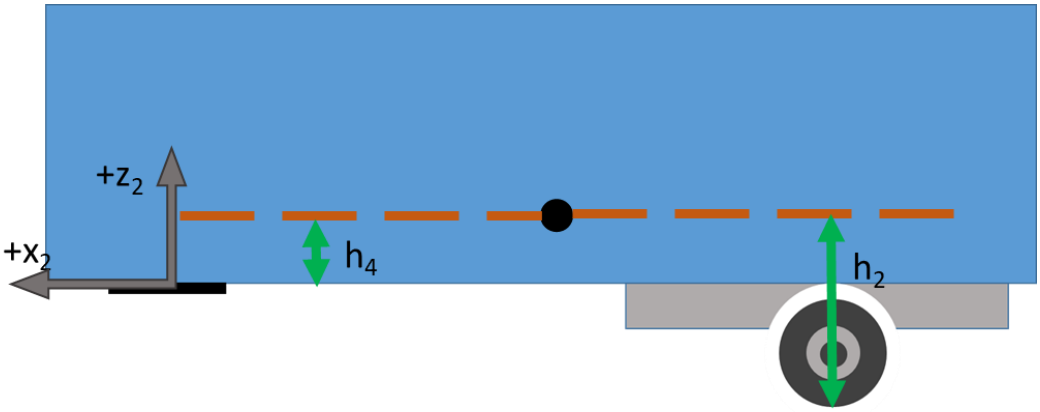

Figure 3.9: Side view of the tractor showing the dimensions of the vehicle.

Figure 3.9 shows the height from the wheel to the CG (h_2) and from the fifth wheel to the CG (h_4).

Using the FBDs and Newton's Laws of Motion, the calculations used to solve for the unknown normal forces, hitch forces, and accelerations are derived. Equations 9 through 20 below show the summing of the forces in the x, y, and z directions for both the tractor along with moment calculations with the assumptions discussed earlier. Equations 12 through 17 are the force summation equations. Since the tractor and trailer have been separated into two FBD, the individual masses have individual force summations. The hitch force is the shared force between them.

$$\sum F_{x1} = m_1 a_{x1} = F_{Hx} - F_{B1} - F_{B23} - F_{rr1} - F_{rr23} - F_{drag} \quad (12)$$

$$\sum F_{x2} = m_2 a_{x2} = -F_{Hx}\cos\Delta + -F_{Hy}\sin\Delta - F_{B451} - F_{B452} - F_{rr451} - F_{rr452} \quad (13)$$

$$\sum F_{z1} = 0 = F_{Hz} + F_{N1} + F_{N23} - m_1 g = F_{Hz} + F_{NR} + F_{NL} - m_1 g \quad (14)$$

$$\sum F_{z2} = 0 = -F_{Hz} + F_{N451} + F_{N452} - m_2 g \quad (15)$$

$$\sum F_{y1} = m_1 a_{y1} = F_{Hy} - F_{C1} - F_{C23} \quad (16)$$

$$\sum F_{y2} = m_2 a_{y2} = -F_{Hy}\cos\Delta - F_{Hx}\sin\Delta - F_{C451} - F_{C452} \quad (17)$$

The moments for the tractor and trailer are shown in Equations 18 through 23. For the x and y moments, the moments were taken about the left rear wheel of the tractor and left wheel of the trailer (wheel 231 and wheel 451, respectively). For the moments around the z-axis, the moments were taken around the CGs of both the tractor and trailer.

$$\sum M_{x231} = 0 = F_{Hz} ww + F_{Hy}(h_1 - h_3) + 2F_{NL} ww - m_1 g ww - m_1 a_{y1} ww \quad (18)$$

$$\sum M_{x451} = 0 = 2F_{N452} ww - F_{Hz} ww - F_{Hx}(h_2 - h_4)\cos\Delta - F_{Hy}(h_2 - h_4)\sin\Delta - m_2 g ww + m_2 a_{y2} h_2 \quad (19)$$

$$\sum M_{y231} = 0 = -F_{Hx}(h_1 - h_3) - 2F_{N1}(L_1 - L_{23}) + m_1 g L_{23} - m_1 h_1 \quad (20)$$

$$\sum M_{y451} = 0 = -F_{Hz}(L_7 - L_{45}) + F_{Hx}(h_2 - h_4)\sin\Delta - F_{Hy}(h_2 - h_4)\cos\Delta - m_2 g L_{45} - m_2 a_{x2} h_2 \quad (21)$$

$$\sum M_{zcg1} = I_1 \ddot{\theta}_1 = -F_{C1} L_1 + F_{C23} L_{23} - F_{Hy} L_6 + ww(F_{BR} - F_{BL} + F_{rrL} - F_{rrR}) \quad (22)$$

$$\sum M_{zcg2} = I_2 \ddot{\theta}_2 = L_{45}(-F_{C451} + F_{C452}) - L_7(F_{Hy}\cos\Delta - F_{Hx}\sin\Delta) + ww(F_{B451} - F_{B452} + F_{rr451} - F_{rr452}) \quad (23)$$

In addition to Newton's Laws, there is a relation between the accelerations in the x-direction due to the hitch coupling the two together. In order to determine this relation, the acceleration for the tractor needs to be related to the acceleration at the hitch then the trailer acceleration can be determined from the hitch acceleration or vice versa. Using Equation 24 shown below, the unknown acceleration of a point on a body can be calculated from a known point [19].

$$a_B = a_A + \alpha \times r_{B/A} + \omega \times (\omega \times r_{B/A}) \quad (24)$$

Translating Equation 24 from the tractor acceleration to the hitch acceleration and from the hitch to the trailer acceleration, Equation 25 below is obtained.

$$a_{x1} - \frac{a_{x2}}{\cos\Delta} = \ddot{\theta}_1(1) L_{45} + (\omega_2(n))^2 L_{45} - \ddot{\theta}_1 L_{23} - (\omega_1(n))^2 L_{23} \quad (25)$$

The angular velocity ω in Equation 25 is calculated using Equation 26.

$$\omega_i = \frac{v}{r_i} \quad (26)$$

For Equation 26, the radius used for the trailer is r_2 calculated using Equation 27. For the tractor Equation XX is used to calculate r_1 which will be used to calculate its angular velocity.

$$r_1 = \sqrt{r_2^2 + L_{23}^2} \quad (27)$$

Using these equations to find the forces and by extension the accelerations including the yaw accelerations, the velocity, angular position, and position can be determined by integrating the accelerations. For greater accuracy, the fourth order Runge-Kutta methodwas used to integrate [20].

With the equations established, the initialization of the forces need to be discussed. The majority of the variables being initialized to zero, several variables including the normal force are not. While these calculations for the initial normal force are simplified and not the most accurate for a vehicle traveling during a turn, they can used to as an initial approximation. Equations28-30 show the three equations used to determine the initial normal forces.

$$F_{N1} = \frac{m_1 g L_{23}}{L_1 + L_{23}} \tag{28}$$

$$F_{N451} = F_{N452} = \frac{m_2 g L_{45}}{2L_{45} + L_7} \tag{29}$$

$$F_{N23} = -F_{N1} - F_{N45} + m_1 g + m_2 g \tag{30}$$

With the initial normal forces, the initial cornering forces are also calculated. The cornering force calculation shall be shown in the Cornering Force section; but with the initial normal force, the cornering force can be solved which will allow the next time step normal force to be solved using a more accurate calculation for a turning vehicle.

In order to perform these calculations more efficiently, a system of linear equations was established to calculate the unknown force and moment equations. As mentioned, the unknowns that the system will solve for are all the normal forces, all the hitch forces, and accelerations in the x-direction. The system of linear equations is solved using Equation 31 and solving for *x*.

$$\mathrm{Ax} = \mathrm{B} \tag{31}$$

In order to solve for *x*, both sides of the equation need to be multiplied by the A^{-1} matrix. For the FBDs shown *A, x,* and *B* are the following matrices:

$$A = \begin{bmatrix} 0 & 0 & 1 & 0 & 0 & 1 & 1 & 0 & 0 & 0 & 0 \\ 1 & 1 & -1 & 0 & 0 & 0 & 0 & 0 & 0 & 0 & 0 \\ 0 & 0 & 0 & -1 & 0 & 0 & 0 & m_1 & 0 & 0 & 0 \\ 0 & 0 & 0 & c_3 & -c_4 & 0 & 0 & 0 & m_2 & 0 & 0 \\ 0 & 0 & 0 & 0 & 1 & 0 & 0 & 0 & 0 & 0 & 0 \\ 0 & 0 & L_7 + L_{45} & -c_1 & c_2 & 0 & 0 & 0 & m_2 h_2 & 0 & 0 \\ 0 & -2ww & ww & c_2 & c_1 & 0 & 0 & 0 & 0 & 0 & 0 \\ 0 & 0 & -ww & 0 & -h_1 + h_3 & 0 & 0 & 0 & 0 & -2ww & 0 \\ 0 & 0 & 0 & h_1 - h_3 & 0 & L_1 + L_{23} & 0 & m_1 h_1 & 0 & 0 & 0 \\ 0 & 0 & 0 & 0 & 0 & 0 & 0 & 1 & -\frac{1}{c_3} & 0 & 0 \\ 0 & 0 & 1 & 0 & 0 & 0 & 0 & 0 & 0 & 1 & 1 \end{bmatrix} \tag{32}$$

Where:

$$c_1 = (h_2 - h_4)\cos\Delta \tag{33}$$

$$c_2 = (h_2 - h_4)\sin\Delta \tag{34}$$

$$c_3 = \cos\Delta \tag{35}$$

$$c_4 = \sin\Delta \tag{36}$$

The A matrix contains all the constants multiplied by the *x* matrix variables shown below in Equation 37. Equation 37 when multiplied by Equation 32 will give Equation 31.

$$x = \begin{bmatrix} F_{N451} \\ F_{N452} \\ F_{Hz} \\ F_{Hx} \\ F_{Hy} \\ F_{N1} \\ F_{N23} \\ a_{x1} \\ a_{x2} \\ F_{NL} \\ F_{NR} \end{bmatrix} \tag{37}$$

With the *A* and *x* matrices holding the unknown variables and the constants that they are multiplied by, the *B* contains the known constants.

$$B = \begin{bmatrix} m_1 g \\ m_2 g \\ -F_{B1}(n) - F_{B23}(n) - F_{drag}(n) - F_{rr1}(n) - F_{rr23}(n) \\ -F_{B241}(n) - F_{B452}(n) - F_{rr451}(n) - F_{rr452}(n) \\ F_{c1}(n) + F_{c23}(n) - m_1 a_{y1}(n) \\ m_2 g L_{45} \\ m_2 a_{y2}(n)(h_2 - h_4) - m_2 g ww \\ m_1 g L_{23} \\ -m_1 g ww - m_1 a_{y1} ww \\ \ddot{\theta}_1(1) L_{45} + (\omega_2(n))^2 L_{45} - \ddot{\theta}_1 L_{23} - (\omega_1(n))^2 L_{23} \\ m_1 g \end{bmatrix} \tag{38}$$

With the equations to solve for the unknown normal forces, accelerations, velocities, and positions established, the other force calculations and descriptions shall now be discussed. The forces that will be covered are the gravitational and normal forces, rolling friction, air drag, brake force, and cornering force.

3.1.2: Gravitational and Normal Forces

Gravitational and normal forces are fundamental throughout all of nature. Every object has a gravitational force. The larger and closer the object is to something, the stronger the gravitational force. The force that is most noticeable and has the greatest effect upon objects near earth is the earth's very on gravitational pull. Newton's Second Law shown below in Equation 39 is the governing equation for calculating gravitational force.

$$F_g = ma = mg \tag{39}$$

Additionally, Newton's Second Law is fundamental to every force equation. *F* represents force, *m* is the mass of the object, *a* is the acceleration of the system, and *g* is the gravitational acceleration. For the tractor-trailer model the *g* used is 9.81m/s^2. The mass of the system is changed for various simulations. Therefore, when both the mass and gravitational acceleration constant are multiplied together, the resulting force is also called the weight.

The normal force is a counter to gravitational force. It counters gravitational force by "pushing" back. For example, a person standing on solid ground does not accelerate down into the ground towards the center of the earth due to the normal force from the ground pushing him

upwards. In a similar fashion, a tractor-trailer no matter how heavy is not going to sink down and accelerate to the core of the earth (assuming the ground is solid enough to support the vehicle weight). The normal force is pushing back against the tire wheels through which the gravitational force pushes down on. Additionally, the normal force is what enables friction (static, kinetic, and rolling friction) which shall now be discussed.

3.1.3: Rolling Friction Force

Rolling friction is the force that opposes the forward motion of the vehicle. Traction enables the wheel to grip the ground and apply wheel torque (which is generated from engine force) to move forward. The rolling friction opposes this traction. The rolling friction and traction are assumed proportional to the normal force. The greater the normal force and by extension the weight, the greater the friction shall be.

Equation 40, shown below, is the rolling resistance force due to friction between the road and the wheels. As the equation shows, the rolling resistance is directly affected the mass of the vehicle.

$$F_{rr} = C_{rr}F_N = C_{rr}F_g \tag{40}$$

With the weight of the vehicle, which was just discussed prior, the only other parameter needed is the coefficient of rolling resistance. For Equation 8, the rolling resistance is set to be 0.01 under dry constant conditions [21]. This force, however, is very small compared to the braking force and, therefore, will not be varied.

3.1.4: Air Drag Force

Air drag force, as the name implies, is the drag (or opposing) force created by the vehicle moving though air. The force has several key factors that affect its magnitude. The frontal area, drag coefficient, and the velocity of the vehicle.

The drag force varies widely between differing vehicles. Due to every vehicle being different in exterior design, the frontal area, which shall be described, is different for every vehicle. Additionally, the drag force is squarely affected by the velocity of a vehicle. The faster a vehicle is traveling, the greater the drag force over the vehicle shall be. Finally, similar to the coefficient of rolling resistance, the drag force has a coefficient of drag. Equation 41 shows the drag force equation [16].

$$F_{drag} = \frac{1}{2}C_d A_f V^2 \tag{41}$$

The frontal area (A_f) is perhaps the most difficult to determine due to every vehicle being different. The frontal area is the area directly hitting the oncoming air as the vehicle moves forward. For class eight tractor-tralers, the frontal area is approximately 6.18 m^2 [21].

The coefficient of drag (C_d) is a constant that reveals how smoothly air moves over the frontal area. If the frontal area is rough the air creates a greater drag over the vehicle. And inversely if the frontal area is polished and smooth the air glides over the vehicle. As an example, a skater on smooth ice can glide easily over the ice versus coarse ice. Similarly air over a polished truck creates less drag. With class eight tractor-trailers, the drag coefficient is approximately 0.654 [21].

Additionally, as the velocity is increased the drag force is squarely increased. The drag force is directly tied to the vehicle and air speed. If the vehicle is not moving there is obviously no drag force on the vehicle. Additionally, if there is a head wind, the vehicle will have a stronger drag force pushing the vehicle back (or a drag force present if the vehicle if it isn't moving). As with the rolling friction, the air drag is also much smaller compared to the braking force.

3.1.5: Brake Force

The braking force is the greatest force in stopping the vehicle. The vehicle (when the brake pedal is applied) will apply pressure to rotors on the wheel to slow down the rotation of the wheels which in turn slows down the vehicle. There are several factors that affect how effectively the vehicle brake force is at slowing the vehicle down. Before discussing these forces, however, seeing how each of these parameters affects the force is shown in Equation 42 [15].

$$F_{brake} = \frac{2}{R}\sum[(p_l - p_o)A_c BF\eta_m \rho f_a f_F r]_i \quad (42)$$

Each of these parameters is specific to the brake used and axle (i) where it is located. Equation 5 is the braking force specific to air brake systems, and each air brake system is going to have its own unique set of parameters while each axle is going to have differing temperatures affecting it. The number of axles not only acts as a means to distribute the weight but also increase the braking force for the vehicle. For purposes of this thesis, the tractor-trailer modeled will be a five axle vehicle with axles 2 and 3 and axles 4 and 5 combined as mentioned in the assumptions.

To begin discussion of the other variables the wheel radius will be considered first. The wheel radius (R which is 0.533 m [15]) has an inverse relationship to the brake force. Therefore, the larger the wheel the harder it is for the vehicle to stop. The brakes of a vehicle do not apply force directly to the wheel. Instead, the brakes apply force to a drum or disc depending on the type. This force is then transferred to the wheel axle as torque which will translate to a force on the wheel. The torque generated by the brake is therefore divided by the wheel radius as shown in Equation 43.

$$F_{brake} = \frac{\tau_{brake}}{R} \quad (43)$$

As mentioned previously, roughly 90% tractor-trailers are equipped with S-cam brakes [15]. These brakes push the brake pads against the drum to create friction and thereby slow down the vehicle. The brake line pressure (p_l) and the pushout pressure (p_o) are the pressure that is in the brake line and the pressure required to begin moving the springs in the brake to move the S-cam in the drum brakes. For the model a pushout pressure of 34473 N/m^2 is used [15].

The brake line pressure, however, is not instantaneous. There is a lag in the system that causes a delay when the brakes are pressed. The delay is caused by the air system needing approximately 0.55 s to reach approximately 90% of pressurization in the line. The brake pressure curve found in Brake Design and Safety [15] shows the time lag from when the air brakes are engaged by the tank to when the brake line has reached peak value.

The brake chamber area (A_c) is the contact area that the brake pad is making with the drum. The contact allows the pressure exerted by the brake pad to be converted to a torque on the axle by friction between the spinning drum and the stationary brake pad. The brake chamber area is set to 0.0187 m^2 [15].

Brake factor (*BF*) is the ratio of the drum drag force over the force that a pad is pressing against the drum. Essentially, it is the ratio of how well the force is transferred from the pad to the drum. The higher the friction the better the factor will be and enable the vehicle to stop quicker [15].

The brake adjustment reduction factor (f_a) is the factor that takes into account the decreased distance the pushrod has moved. For the model, a factor of 1.0 was used for all brakes [15].

Temperature additionally plays an adverse effect on braking. The brake temperature fade reduction factor (f_F) is the effect that temperature plays on braking. As the temperature of the brakes increases, the coefficient of friction between the brake pads and drum lessens. Therefore, the less friction between the pad and drum causes severe problems in braking. For this simulation, the reduction factor is assumed to be held constant and at 0.70. However, in practice, the reduction factor follows the below equations (Equations 44 and 45) (where *T* is the temperature of the brakes) (both equation from [15]:

$$f_F = 1 \; when \; T \leq 366 \; K \tag{44}$$

$$f_F = 1 - 0.00058T \; when \; T \; > 366 \; K \tag{45}$$

Next is the drum radius (*r*). As what has been discussed with the brakes creating a torque on the axle of the wheel, the radius of the drum is what allows this. Since the brake pads are applying a force to the drum, this is translated to the axle through the effective radius of the drum. Therefore, the greater the radius of the drum, the greater the torque on the axle. The drum radius is set to 0.2032 m for the model [15].

Due to losses from mechanical efficiency, the term η_m is used to represent the effectiveness of the system. Varying brake systems can have higher or lower efficiency. For the brakes modeled, the efficiency is 0.7. Efficiency losses arise from heat or sound produced by a system. In the case of braking, causing contact and friction between the pads and drum not only creates the desired opposing torque but also heat and some noise. In the case of the modeled brakes, 30% of the energy used by the system to create the friction is lost to heat and noise. The more efficient the system, the lower the heat or noise produced will be [15].

The final variable is the lever ratio (ρ) of the pushrod and pad. The pushrod presses up against a lever which turns the cam which pushes the brake pads outward. Equation 46 shows the lever ratio formula for s-cam brakes.

$$\rho = \frac{l_s}{2l_c} \tag{46}$$

For S-cam brakes (which is what is modeled), the effective cam radius (l_s) and effective slack length (l_c) dictate the value of the lever ratio. The cam radius and slack length are 1.27 cm and 0.38 cm, respectively. While discussion of the brakes has been focused on drum brakes, it is important to note that simply changing the lever ratio to 15.8 will allow the user to model disc brakes as well [15]. For this thesis, both drum and disc brakes will be modeled to observe the differences. The potential difference shall now be explored.

3.1.5.1: Brake Type Comparison

The purpose of choosing disc brakes as a comparison is due to disc brakes being known to be able to handle heat better than drum brakes. The,

"physical advantage of disc brakes is that the inevitable thermal expansion causes the ferrous brake surface to expand – this is disadvantageous for drums, since expansion moves the braking surface away from the pad, better for discs, forcing the metal disc into the pad." [25]

Due to heat causing the brakes to expand, having the brakes expand to cause greater braking force instead of failure is the appropriate route to take. Additionally, disc brakes are also shown to have greater "consistency" over drum brakes [25]. Having a braking system that is repeatable and reliable is crucial for an autonomous system. If a failure occurs on a brake level in an autonomous vehicle, catastrophic results may occur.

Since disc brakes handle thermal expansion better than drum brakes, the final issue and comparison of jackknifing, therefore, remains. In order to prevent jackknifing, the trailer must either be controlled or exert a greater stopping force compared to the tractor. Correcting for jackknifing by maintaining control over the vehicle, therefore, may require changing the braking system of the vehicle from drum to disc.

Dunn et al. simulated a tractor-trailer stopping during a turn using TruckSim™. The tractor-trailer was simulated under various road conditions of medium and low road friction (μ), under no load and half the gross vehicle weight (GVW) (maximum vehicle weight with load), with automatic braking system (ABS) on and off, with half and full treadle (brake line pressure), and either drum/drum or disc/drum brakes on the tractor and trailer, respectively. Table 3.1 shows the yaw rates in degrees/sec of the tractor simulated by Dunn et al. [25].

Table 3.1: Simulation results simulated by Dunn et al. of tractor-trailer yaw stability. The red boxes indicate a jackknifing in the simulation. The yellow boxes indicate the vehicle almost jackknifed. Results pulled directly from Dunn et al. [25].

		No Load				½ GVW Load			
		Medium μ (μ~0.55)		Low μ (μ~0.30)		Medium μ (μ~0.55)		Low Medium μ (μ~0.30)	
		Drum / drum	Disc / drum	Drum / drum	Disc / drum	Drum / drum	Disc / drum	Drum / drum	Disc / drum
Half Treadle	Full ABS	6.9	6.2	5.8	5.6	7.2	6.7	7.5	6.7
	No ABS	49.7	19.3	4.7	2.2	50.9	34.9	7.8	2.6
Full Treadle	Full ABS	6.4	6.6	6.0	6.2	6.9	6.4	7.5	7.6
	No ABS	8.8	3.5	2.0	1.2	12.5	6.0	2.3	1.3

In nearly every case, the tractor has a decreased yaw rate with disc brakes on the tractor. Additionally, there is only one case where the disc/drum brake combination experienced jackknifing; whereas, the drum/drum brake combination experienced two jackknifes and three near jackknifing events. What is to be noted in the simulations, however, is that the drum brakes are

not modeled for thermal expansion. While the brakes may be performing well at full brake line pressure in the simulations, they may experience further failure due to heat in real world applications.

Finally, the comparison between the brakes stopping distances were made using a study from NHTSA. The study conducted by Dunn and Hoover in 2004, testing was performed on tractor-trailers equipped with drum and/or disc brakes. Dunn and Hoover conducted the study to determine the best brakes that meet the FMVSS No. 121 stopping standards. The group used the following brake configurations:

1. All s-cam drum brakes
2. Hybrid Drum: Large capacity s-cam drum on the front axle and regular s-cam on the remaining axles
3. Hybrid Disc: Air disc on the front axle and s-cam on the remaining axles
4. All air disc brakes

In addition to testing these four brake configurations, the group also tested these brake sets on two different tractor. The tractor used were Peterbilt and Volvo tractors. The tractors were also tested loaded up to 50,000lb and unloaded at 20,460 lb (Peterbilt) and 19,070 lb (Volvo) [26]. Table 3.2 shows the stopping distances of the tractor-trailers with the different brake configurations obtained by Dunn and Hoover [26].

Table 3.2: Dunn and Hoover tractor-trailer stopping distances using various brake configurations. Information from Dunn and Hoover [26]

	Unloaded		Loaded	
Brake Type	Mean Stopping Distance (m) (Peterbilt)	Mean Stopping Distance (m) (Volvo)	Mean Stopping Distance (m) (Peterbilt)	Mean Stopping Distance (m) (Volvo)
All S-cam Drums	70.1	64.6	96.6	80.5
Hybrid Drums	58.5	62.5	76.8	82.0
Hybrid Disc	54.3	55.2	75.3	80.2
All Disc	55.2	57.3	67.7	73.5

Table 3.2 shows that if the tractor-trailer is to be loaded, the best stopping distance results are acquired with all disc brakes on the axles. Drum brakes performed the worst in both unloaded and loaded tests. Even in an unloaded configuration, the tractor-trailer performs significantly better with disc brakes on the tractor (hybrid disc). It is recommended, therefore, to place disc on all axels even though the stopping distances are slightly longer compared to hybrid disc in the unloaded weight due to the better performance loaded.

The work conducted by this research will also seek to perform similar simulations to Dunn et al. and Dunn/Hoover. The results obtained in Dunn and Hoover will be by which the stopping distance with different brakes is matched to. Then the turning stopping distance stability will be compared to Dunn et al.

In the three categories that have been discussed, heat management, jackknifing, and stopping distance, tractor-trailers perform significantly better with the presence of disc brakes. It is recommended, therefore, that an autonomous tractor-trailer to maintain safety, stability, and consistency stopping have disc brakes at least the tractor if not over the entire vehicle.

3.1.6: Cornering Force

When a vehicle is traveling through a curve or turn, the cornering force is the force at the tire caused by tire slip that opposes the centripetal acceleration and will help prevent the vehicle from being pushed out or pulled to a turn largely due to the corning force. In addition to preventing the vehicle from being pulled into or out of a turn, the cornering force helps the trailer of a tractor-trailer to not jackknife. When the cornering force on the trailer begins to saturate, the trailer can jackknife or slide out of control [18]. While the cornering force can be simplified to a linear relationship with the normal force, it was important for this model to have a more accurate cornering force for jackknifing simulations. The cornering force can be calculated using the following equation [18]:

$$F_c = 2\mu F_N\left(\frac{C_r \tan\alpha}{\mu F_N} - \frac{1}{3}\left(\frac{C_r \tan\alpha}{\mu F_N}\right)^2 + \frac{1}{27}\left(\frac{C_r \tan\alpha}{\mu F_N}\right)^3\right) \quad (47)$$

In Equation 47, the cornering force is calculated from the normal force (F_N), the cornering stiffness (C_r), the coefficient of friction between the tire and road (μ), and the tire slip angle (α). The cornering stiffness is constant through the simulation which is set to 8000. The coefficient of friction is set from .3 to .8 (for different simulations to simulate wet and dry roads) [20]; the slip angle and normal force are calculated for each time step at the different wheel sets.

Using Equation 47, the cornering force at each wheel or set of wheels can be determined. The cornering force, however, cannot be solved linearly using the linear solver provided by MATLAB®. The method chosen to solve for the cornering forcer, therefore, is to first determine the initial normal force, determine the initial cornering force, calculate the next time step normal force, then solve for the next time step cornering force, and continuing this process until the simulation is over.

3.2: MATLAB® Model

Now that the equations have been determined and discussed, the model can now be shown. In order to create the model, MATLAB® 2017a was used. The usage of MATLAB® allowed for easier visualization, time simulations, and acquiring multiple simulations quickly. Additionally with MATLAB®, calculations can be made quickly for each parameter change versus doing hand calculations.

The following discussion is a section by section break down of the MATLAB® code created for the tractor-trailer model. The full code can also be seen in Appendix A without the comments. The code contains three different loops. The first two for loops are used to simulate the changing steering angles and changing trailer cg locations. The final loop is a for loop for the

changing time. The time loop changes the time by the desired time step. In the time loop, the position, velocity, and force calculations occur.

The following several segments of the code are dedicated to defining the vehicle parameters such as distances between the axles and CG, the weights, braking parameters, coefficients of friction and rolling friction, and cornering stiffness.

```
%Initalizing the tractor, trailer, and other variables
h1 = 1.4;       %height from the bottom of the wheel to the tractor cg (m)
h2 = 1.5;       %height from the bottom of the wheel to the trailer cg (m)
h3 = .5;        %height from the fifth wheel to the tractor cg (m)
h4 = .8;        %height from the fifth wheel to the trailer cg (m)
I1 = 400000;    %moment of inertia of the tractor kg*m^2
I2 = 767667;    %moment of inertia of the trailer kg*m^2
g = 9.81;       %gravity constant m/s^2
W1 = 20000*4.448;   %weight of the tractor (N)
W2 = 100000*4.448;  %weight of the trailer (N)
m1 = W1/g;          %determining the mass of the tractor (kg)
m2 = W2/g;          %determining the mass of the trailer (kg)
ww = 2.6/2;         %distance from the axle to the wheel (m)

%Braking Parameters
R = 21*.0254;       %Wheel radius (m)
roeL = 90*6894.76;  %Brake line pressure (N/m^2)
roeo = 5*6894.76;   %Pushout pressure (N/m^2)
roe = 5.5;          %Lever ratio
Ac = 28*.00064516;  %Brake chamber area (m^2)
BF = 1.3;           %Brake factor
mum = .7;           %Mechanical efficiency
fa = .85;           %brake adjustment reduction factor
fF = .7;            %brake temperature fade reduction factor
r = 8*.0254;        %drum rotor radius (m)


Cf = 8000;          %Cornering force
u = .8  ;           %Coefficient of friction


%Tractor parameters
L1 = 2.59;              %Distance from front axle to the cg
L6 = 3.36;              %Distance from fifth wheel to the cg
L23 = 2.7+(4.02-2.7)/2; %Distance from the rear axle to the cg
```

Next is the initialization of the hitch, brake, and cornering forces. Additionally, before the first for loop begins, the time step and storage variable are declared.

```
%Initailizing the Hitch, Brake, and Cronering forces.
FHX(1) = 0;
FHY(1) = 0;
FHZ(1) = 0;
FB1(1) = 0;
FB23(1) = 0;
FB45(1) = 0;
FC1(1) = 0;
FC23(1) = 0;
FC451(1) = 0;
```

```
FC452(1) = 0;

degrad = pi/180; %conversion from degrees to radians
raddeg = 180/pi; %conversion from radians to degrees


%Setting the time step and the "b" storage variable
dt = .05;
delay = 0.5;
b = 1;
```

With the majority of the variable declared, the first for loop is declared. This for loop allows multiple simulations to be run stepping though different steering angles. Depending on the users desires, a wide range of steering angles can be observed and the affect these steering angles will have on the vehicle can be observed.

```
%The first for loop steps through different steering angles "stang1". The
%steering angle steps from 0.0001 deg to the desired final angle.


for alpha1 = 0.0001*degrad:.1*degrad:5*degrad


   %Setting the storage variables to one for each loop
   a = 1;
   n = 1;
```

Nested within the first for loop is the second for loop. For each steering angle the first for loop has, the second for loop will sweep through the user defined trailer CG location. As with the steering angle, the user can sweep through a wide range of trailer CG locations to observe the affect this parameter has on jackknifing and stopping distance.

```
%For each steering angle the trailer cg location (tcg) is moved as
%desired be the user. The trailer cg location is shifted by 0.1m for
%each loop.
for tcg = 3:.1:5
```

For each loop run, the variable need to be cleaned from the previous run values. Clearing the variables ensures that the previous run values will not be recorded or affect the next run. After the variables are cleared, the initial values are set for the velocity, acceleration, and position variables.

```
%After each loop the variables again need to be cleard so that the
%proper values are calculated and stored
clearvars v s vangle1 vangle2 sangle1 sang2 ...
   time ay1 ay2 ax1 ax2 AngDiff

%Declairing the variables for the trailer cg location between the
%fifth wheel and rear axle.
L7 = tcg;        %Distance from the hitch to the cg
L45 = 5.2450-tcg; %Distance from the trailer axle to the cg

%Determinig the turning radius for the tractor (r1) and trailer
```

```
%(r2)
r2 = (L23+L1)/(tan(alpha1))+(ww); %turning radius of the trailer m
r1 = sqrt((power(r2,2)+power(L23,2))); %turning radius of the tractor m


%Setting up the initial values that will need to be cleared after
%each simulation.
FN1(1) = m1*g*L6/(L1+L6);
FN45(1) = m2*g*L45/(L45+tcg);
FN451(1) = FN45(1)/2;
FN452(1) = FN45(1)/2;
FN23(1) = -FN1(1)-FN45(1)+m1*g+m2*g;
FNL(1) = FN23(1)/2+FN1(1)/2;
FNR(1) = FN23(1)/2+FN1(1)/2;
v(1) =  70*0.44704; %initializing velocity m/s
th1(1) = 0;        %initializing tractor yaw acceleration rad/s^2
th2(1) = 0;        %initializing trailer yaw acceleration rad/s^2
vangle2(1)=0;      %initializing tractor yaw velocity rad/s^2
vangle1(1)=0;      %initializing trailer yaw velocity rad/s^2
s(1) = 0;          %initializing the position to zero m
ax1(1) = 0;        %initializing the tangental acceleration of the tractor m/s^2
ax2(1) = 0;        %initializing the tangental acceleration of the trailer m/s^2
ay1(1)=power(v(1),2)/r1; %initializing the centripital acceleration of the tractor
m/s^2
ay2(1)=power(v(1),2)/r2; %initializing the centripital acceleration of the trailer
m/s^2
sangle1(1)= 0;     %initializing the tractor angle to zero rad
sang2(1)=asin((L7+L45)/(power(r2,2))); %initializing the trailer
                %angle relative to the tractor given steering
                %angle, fifth wheel position, and cg positions
FC1(1) = 2*u*FN1(1)*(((Cf*tan(sangle1(1)))/(u*FN1(1)))-(1/3)...
      *power(((Cf*tan(sangle1(1)))/(u*FN1(1))),2)+(1/27)...
      *power(((Cf*tan(sangle1(1)))/(u*FN1(1))),3));
FC23(1) = 2*u*FN23(1)*(((Cf*tan(sangle1(1)))/(u*FN23(1)))-(1/3)...
      *power(((Cf*tan(sangle1(1)))/(u*FN23(1))),2)+(1/27)...
      *power(((Cf*tan(sangle1(1)))/(u*FN23(1))),3));
FC451(1) = 2*u*FN451(1)*(((Cf*tan(sang2(1)))/(u*FN451(1)))-(1/3)...
      *power(((Cf*tan(sang2(1)))/(u*FN451(1))),2)+(1/27)...
      *power(((Cf*tan(sang2(1)))/(u*FN451(1))),3));
FC452(1) = 2*u*FN452(1)*(((Cf*tan(sang2(1)))/(u*FN452(1)))-(1/3)...
      *power(((Cf*tan(sang2(1)))/(u*FN452(1))),2)+(1/27)...
      *power(((Cf*tan(sang2(1)))/(u*FN452(1))),3));


%Declaing the storage vairable n and time variable for each run
%through the for loop
n = 1;
time(1) = 0;
```

Finally, within the second for loop is the last for loop. The final loop steps through the desired time step calculating the forces, accelerations, velocities, and distance. This for loop has

an if statement embedded within it to check the velocity value. Once the velocity value has reached zero, the calculations will end.

```
%The last for loop is the simulation of the tractor-trailer
%traveling from the initial velocity to zero. The loop is set up to
%step through the desired time step until the velocity reaches
%zero.
 for t=0:dt:600
   %The if statement is established to break the simulation when
   %the velocity of the tractor-trailer reaches zero
    if v(n)>0

     %Determing the angular velocity for each time step
     w1 (n) = v(n)/r1; %angular velocity of the tractor (rad/s)
     w2 (n) = v(n)/r2; %angular velocity of the trailer (rad/s)
      Fdrag(n) = .5*cd*Af*power(v(n),2);
      Frr1(n) = crr*FN1(n);
      Frr23(n) = crr*FN23(n);
      Frr451(n) = crr*FN451(n);
      Frr452(n) = crr*FN452(n);
      FrrL(n) = crr*FNL(n);
      FrrR(n) = crr*FNR(n);
```

Within the time loop, are the calculations for solving for the *x* matrix. This calculations is performed every step to determine the normal forces, hitch forces, and accelerations. Using MATLAB®'s function "linsolve" the *x* matrix can be solved by multiplying the *A* inverse matrix to the *B* matrix. This function only works linearly so the cornering force will be calculated next for the next time step.

```
%Here the matricies A and B are set up to solve for x in the
%Ax=B using MATLAB®'s linear solver (linsolve). The x being
%solved for are the unknown normal forces, hitch forces, and
%tangental accelerations. The A matrix contains the constants
%being multiplied to the x variables. The B matrix has the
%known constants.

%Setting up varaiables for the A matrix
 c1 = (h2-h4)*cos(sang2(n));
 c2 = (h2-h4)*sin(sang2(n));
 c3 = cos(sang2(n));
 c4 = sin(sang2(n));

%Setting up the A matrix. The comments at the top show which
%collums represent which unknown variables.
 %FN451 FN452  FHZ     FHX FHY      FN1 FN23  ax1  ax2
A0 =[1,    1,   -1,      0,  0,       0, 0,   0,    0;... %sum z2
    0,    0,(L6+L45), -c1, c2,       0, 0,   0,m2*h2;... %My 451
    0,-2*ww,   ww,     c2, c1,       0, 0,   0,    0;...  %Mx 451
    0,    0,    1,      0,  0,       1, 1,   0,    0;... %sum z1
    0,    0,    0,(h1-h3),  0,(L1+L23), 0, m1*h1,  0;... %My 231
    0,    0,    0,      0,  1,       0, 0,   0,    0;...%sum y1
    0,    0,    0,     c3,-c4,       0, 0,   0,   m2;... %Sum x2
    0,    0,    0,     -1,  0,       0, 0,  m1,    0;... %Sum x1
```

```
    0,   0,   0,     0,  0,      0, 0,   1,   -1];   %ax1 and ax2 relationship

 %Establishing the B matrix with the known variables.
B0 = [m2*g;...                  %Sum z2
   -m2*g*L45;...                %My 451
   m2*ay2(n)*(h2-h4)-m2*g*ww;...  %Mx 451
   m1*g;...                     %Sum z1
   m1*g*L23;...                 %My 231
   FC1(n)+FC23(n)-m1*ay1(n);...   %Sum y1
   -FB45(n);...                 %Sum x2
   -FB1(n)-FB23(n);...          %Sum x1
   th2(n)*L45+power(w2(n),2)*L45-th1(n)*L23-power(w1(n),2)*L23]; %ax1 and ax2
relationship

%Using linsolve, the x variables are being solved for in
%A^-1*A*x=A^-1*B
F0 = linsolve(A0,B0);

%From F0, the individual variables can be pulled.
FN451(n) = F0(1,1);    %Wheel 451 Normal Force (N)
FN452(n) = F0(2,1);    %Wheel 452 Normal Force (N)
FHZ(n) = F0(3,1);      %Hitch force in the z direction (N)
FHX(n) = F0(4,1);      %Hitch force in the x direction (N)
FHY(n) = F0(5,1);      %Hitch force in the y direction (N)
FN1(n) = F0(6,1);      %Tractor Front Normal Force (N)
FN23(n) = F0(7,1);     %Tractor Rear Normal Force (N)
ax1(n+1)=F0(8,1);      %Tractor tangental acceleration (m/s^2)
ax2(n+1)=F0(9,1);      %Trailer tangental acceleration (m/s^2)
```

With the normal forces calculated, the cornering force can be determined. The cornering forces calculated here will be used for the next time step calculations for the normal forces, hitch forces, and accelerations.

```
%Cornering Force Calculations for the tractor
if sangle1(n)== 0 %Setting the corning force to zero  when the angle is zero
   FC1(n+1) = 0;
   FC23(n+1) = 0;
%calculating the corning force for the tractor angles other than zero.
else
   FC1(n+1) = 2*u*FN1(n)*(((Cf*tan(sangle1(n)))/(u*FN1(n)))-(1/3)...
 *power(((Cf*tan(sangle1(n)))/(u*FN1(n))),2)+(1/27)*power(((Cf*tan(sangle1(n)))/(u*FN1(n))),3));

   FC23(n+1) = 2*u*FN23(n)*(((Cf*tan(sangle1(n)))/(u*FN23(n)))-(1/3)...
*power(((Cf*tan(sangle1(n)))/(u*FN23(n))),2)+(1/27)*power(((Cf*tan(sangle1(n)))/(u*FN23(n))),3));
end

%Cornering Force Calculations for the trailer
if sang2(n) == 0 %Setting the corning force to zero  when the angle is zero
   FC451(n+1) = 0;
   FC452(n+1) = 0;
%calculating the corning force for the trailer angles other than zero.
else
   FC451(n+1) = 2*u*FN451(n)*(((Cf*tan(sang2(n)))/(u*FN451(n)))-(1/3)...
*power(((Cf*tan(sang2(n)))/(u*FN451(n))),2)+(1/27)*power(((Cf*tan(sang2(n)))/(u*FN451(n))),3));
   FC452(n+1) = 2*u*FN452(n)*(((Cf*tan(sang2(n)))/(u*FN452(n)))-(1/3)...
*power(((Cf*tan(sang2(n)))/(u*FN452(n))),2)+(1/27)*power(((Cf*tan(sang2(n)))/(u*FN452(n))),3));
```

```
end
```

Next to be calculated are the brake forces. The brake force calculations are nested within a if statement. This if statement is where the delays come into effect. The brakes are only fully applied not only when the brake line pressure is reached, but also when the "processing" time has elapsed and the software has recognized the object. In addition to a delay, the brake forces are also limited in how much force they can apply to the wheel by the weight applied to that wheel times the coefficient of friction [27].

```
%Calculating the braking force. The braking force starts at
%0.5 seconds due to the brake line pressure requiring build
%up pressure.
if t >= .5
   FB1(n+1) = (2/(R))*((roeL-roeo)*(Ac*BF*mum*roe*fa*fF*r));
   FB23(n+1) = (2/(R))*((roeL-roeo)*(Ac*BF*mum*roe*fa*fF*r));
   FB45(n+1) = (2/(R))*((roeL-roeo)*(Ac*BF*mum*roe*fa*fF*r));
else
   FB1(n+1) = 0;
   FB23(n+1) = 0;
   FB45(n+1) = 0;
end


%Perfomring a check on the braking force. The braking force
%cannot exceed the normal force multiplied by the
%coefficient of friction.

%Checking the brake force at the front tractor axle
if FB1(n+1) > u*FN1(n)
      FB1(n+1) = u*FN1(n);
end
%Checking the brake force at the rear tractor axle
if FB23(n+1) > u*FN23(n)
      FB23(n+1) = u*FN23(n);
end
%Checking the brake force at the trailer axle
if FB45(n+1) > u*(FN451(n)+FN452(n))
      FB45(n+1) = u*(FN451(n)+FN452(n));
end
```

With all the necessary calculations complete, the accelerations in the y-direction and the yaw accelerations can be calculated. When the calculations are complete, the velocity and position calculations are performed using a Runge-Kutta integrator. This integrator is in a function shown next.

```
%Solving the final unknowns for the tractor and trailer
%centripital acceleration and yaw acceleration.
ay2(n+1) = (-FC451(n+1)-FC452(n+1)-cos(sang2(n))*FHY(n)...
   -sin(sang2(n))*FHX(n))/m2;
th2(n+1) = (FC451(n+1)*L45+FC452(n+1)*L45-cos(sang2(n))...
   *FHY(n)*L7-sin(sang2(n))*FHX(n)*L7)/I2;
ay1(n+1) = (-FC1(n+1)-FC23(n+1)+FHY(n))/m1;
th1(n+1) = (-FC1(n+1)*L1+FC23(n+1)*L23-FHY(n)*L6)/I1;

%Storing the time
```

```
        time(n+1)=t;

        %Using the runge-kutta method to integrate the acceleration
        %to acquire the next velocity value and to integrate the
        %velocity to acquire the next position value.
        v(n+1) = integrator(ax1(n),v(n),dt);
        s(n+1) = integrator(v(n),s(n),dt);
        vangle1(n+1) = integrator(th1(n),vangle1(n),dt);
        sangle1(n+1) = integrator(vangle1(n),sangle1(n),dt);
        vangle2(n+1) = integrator(th2(n),vangle2(n),dt);
        sang2(n+1) = integrator(vangle2(n),sang2(n),dt);

        n=n+1;
    end
end
```

The Runge-Kutta developed below was created using a function developed by Ido Schwartz [28].

```
function [ y ] = integrator( x,yi,step )
%   The purpose of this function is to integrate the x value using the
%   runge kutta method.

F_x = @(x) x;

    k_1 = F_x(x);
    k_2 = F_x(x+0.5*step);
    k_3 = F_x((x+0.5*step));
    k_4 = F_x((x+step));

    y = yi + (1/6)*(k_1+2*k_2+2*k_3+k_4)*step;  % main equation
end
```

With all of the calculations complete, the values found can now be stored for plotting later. The values being stored are the steering angles used, the trailer CG locations used, the angles of the tractor and trailer relative to each other, and the stopping distance calculated.

```
%Storing the runs for plotting
Delta (a) = tcg;        %Storing the steering angle
srungeA (a) = s(end); %Storing the distance taken to stop
SA1(a) = sangle1(n);       %Storing the angle of the tractor
SA2(a) = sang2(n);       %Storing the angle of the trailer


%Within this for loop, the program compares the angle of the
%tractor to the trailer to determine the difference at each time
%step
for x = 1:1:n
   AngDiff(x) = abs(abs(sangle1(x))-abs(sang2(x)));
%        if AngDiff(x)> 45*drad
%           AngDiff(x) = 45*drad;
%        end
end
```

```
        %After performing the comparison, the program determines what the
        %largest difference was using the "max" function
        AngDiffMax(a) = max(AngDiff);
        va2(a) = max(vangle2);

        %Changing the a value for the next set of iterations for the
        %changing trailer cg location
        a = a+1;
    end

    %Outside of the for loop for the changing trailer cg location, the
    %values obtained for the steering angle, stopping distance, tractor
    %angle, trailer angle, the angle difference between the tractor and
    %trailer are stored in the vector or cells below.

    angle(b) = alpha1;      %Storing the steering angle
    distance{b} = srungeA;  %Storing the stopping distance
    Ang1 {b} = SA1;         %Storing the tractor angle
    Ang2 {b} = SA2;         %Storing the trailer angle
    AngD {b} = AngDiffMax;  %Storing the maximum angle difference between the tractor and
trailer
    VA2 {b} = va2;          %Storing the trailer angular velocity
    cg {b} = Delta;         %Storing the cg position

    %Stepping the storage variable
    b = b+1;
end
```

Once all of the calculations and loops are complete, the code will then plot the stopping distance and max angle between the tractor and trailer over the steering angle and trailer CG location to create 3D plots.

```
%converting the cells to be plotted
dis = reshape(cell2mat(distance),[],length(distance));
cgdis = reshape(cell2mat(cg),[],length(cg));
A2 = reshape(cell2mat(Ang2),[],length(Ang2));
A1 = reshape(cell2mat(Ang1),[],length(Ang1));
AD = reshape(cell2mat(AngD),[],length(AngD));
VA2 = reshape(cell2mat(VA2),[],length(VA2));

figure
mesh(angle*raddeg,cgdis,dis)
hold on
xlabel ('Steering Angle (deg)')
ylabel('CG Location (m)')
zlabel('Stopping Distance (m)')
hold off

figure
% mesh(angle*radd,cgdis,A2*radd)
% mesh(angle*radd,cgdis,A1*radd)
mesh(angle*raddeg,cgdis,AD*raddeg)
hold on
xlabel ('Steering Angle (deg)')
ylabel('CG Location (m)')
zlabel('Trailer Final Angle (deg)')
```

```
hold off
```

With the presentation of the code complete, the results obtained were then displayed. While the results will sweep through the steering angles and trailer CG locations, the entire code would need to be run for changing other parameters such as weight or brake parameters.

Chapter 4: Results

Now that the model has been fully discussed and parameters properly set, the stopping distances can now be determined. Before the results are shown, however, it is crucial to verify with outside sources if the proper calculations are being made and if the model will accurately show us previously unknown results. After the stopping distances and max angle between the tractor and trailer will be plotted against the vehicle's varying weights, brake type, and speeds will to determine the trends.

4.1: Verification of Results

Before looking at results, the braking model was first parameterized to match the results from experiments conducted by the Dunn and Hoover study [26]. The initial speed, weight, and brake types were set match those of Dunn and Hoover, the results in Table 4.1 show how closely the simulation was refined to match the study. A range of $\pm 1^{o}$ was used for all the runs to simulate any small corrections a driver may be making for a "straight" line stop. Additionally since it is unclear where the trailer is loaded, the trailer CG is shifted from 2.5 – 4 m from the fifth wheel. For the loaded simulation, the model was set to a total weight of 50,000 lb. With the results from the steering angle range and trailer CG location, the average stopping distance was calculated. Table 4.1 shows these averages compared to the study.

Table 4.1: Validation of Simulations to results from Dunn and Hoover [26]

Brake Type	**Mean Stopping Distance (Peterbilt) (m)**	**Mean Stopping Distance (Volvo) (m)**	**Simulation (m)**
All S-cam Drums	96.6	80.5	93.0
All Disc	67.7	73.5	67.7

While these simulations closely match the results Dunn and Hoover, it is important for the end user to verify results and parameters if the wish is to model different brakes or trucks. The results shown next are based off of the matching of the tractors in the Dunn and Hoover study.

4.2: Simulation Results

For the simulations conducted for this research, several parameters were varied to study how the parameters would affect the tractor-trailer stability and stopping distance (excluding the braking parameters that were set to match the Dunn and Hoover study). For these simulations, a 0.55 software processing delay was added. This delay was added in addition to the time required for the brakes to become engaged. In addition to the changing trailer CG location and the steering angle, the tractor-trailer will also be simulated at different coefficients of friction, trailer weight, and drum or disc brakes. By varying these parameters, the end user can better select the brakes, trailer loading, and safe driving conditions in inclement weather. The purpose of these simulations is to show the effects the parameters have on the trailer angle and stopping distance. The plots captured are to be used as a tool and example for the end user. The 3D plots can be used to show a region of operation that is safe for the vehicle to operate within. If however, spikes or large trailer angles are noticed on the plots, the end user can now that a jackknifing event occurs at these conditions.

Within this section, a tractor-trailer with a total weight of 80,000 lb (20,000 lb tractor and 60,000 lb trailer), varying coefficient of friction from 0.3 and 0.8, an initial velocity of 70 mph, and drum and disc brakes. The parameters covered in the simulations are presented in Table 4.2. The plots covered in this chapter are highlighted in blue, and a summary table of all the simulations shall be shown at the end of the chapter.

Table 4.2: Parameters varied over simulations.

Delay (sec)	0.55															
Weight	50,000								80,000							
Brake Type	Drum				Disc				Drum				Disc			
Coefficient of Friction	0.3		0.8		0.3		0.8		0.3		0.8		0.3		0.8	
Initial Speed	60	70	60	70	60	70	60	70	60	70	60	70	60	70	60	70

In order to first demonstrate how the regions of operation are obtained, the first set of plots shown in Figure 4.1 through Figure 4.4 cover a wide range of steering angles and trailer CG locations. These plots show peaks where the tractor-trailer is considered to be jackknifing. When observing these plots, the user can narrow the parameters to find the appropriate regions of operation by looking at the planes in these plots. Figure 4.1 through Figure 4.4 shows the process of narrowing down the operating parameters to the region of operation by reducing the steering angle and/or trailer CG location.

For Figure 4.1 through Figure 4.4, the simulation parameters are set to a total weight of 80,000 lbs, drum brakes, coefficient of friction of 0.8, and initial velocity of 70 mph. This process is the same process that will be used for later simulations with different parameters.

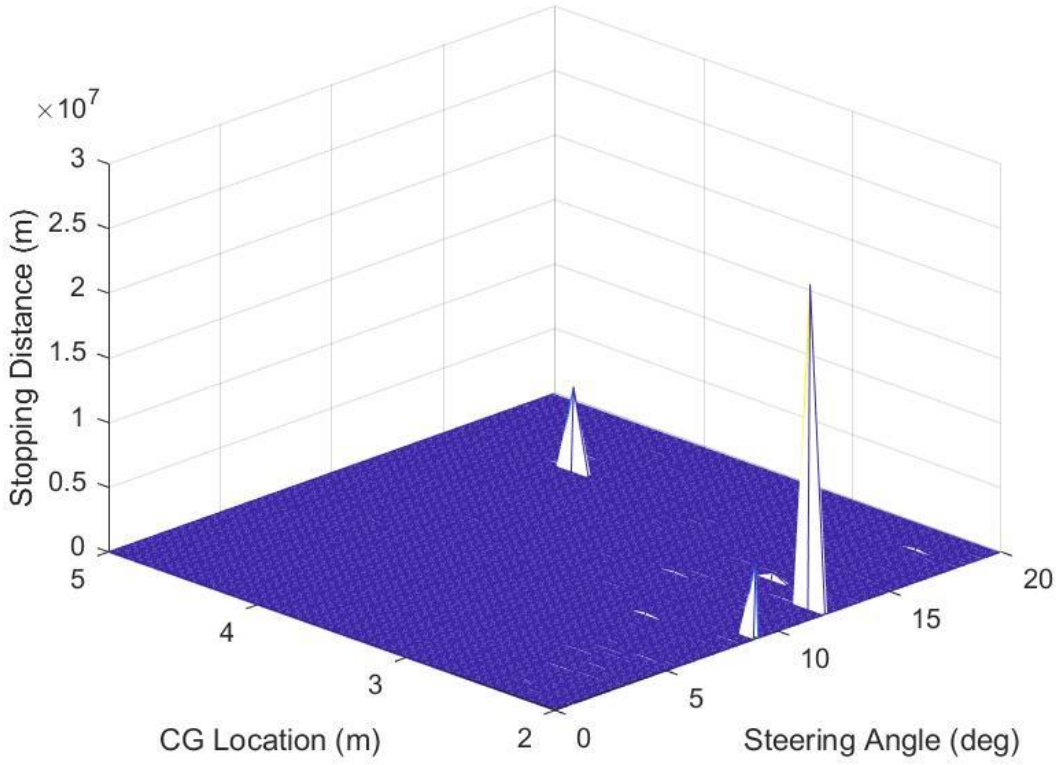

Figure 4.1: First simulation showing peaks of jackknifing. The plane shows areas where the tractor-trailer can be operated safely. Narrowing will help prevent jackknifing.

The second simulation shows the region of operation narrowed down to a trailer CG location of 2-5 m with the same steering angle range.

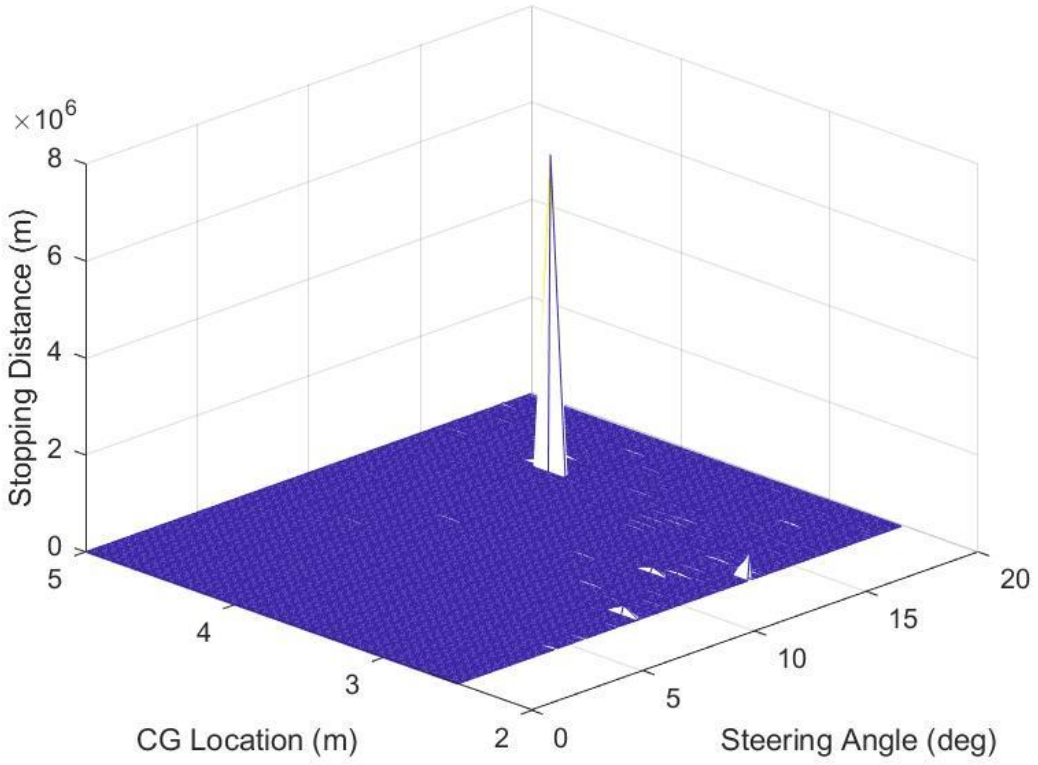

Figure 4.2:The second run again shows jackknifing peaks but of a lesser magnitude. Reducing the region of operation again will help to further remove these instances.

Reducing the region of interest to a trailer CG location of 2.5-5m and 0-10 degrees steering angle, Figure 4.3 shows the third run with these new ranges.

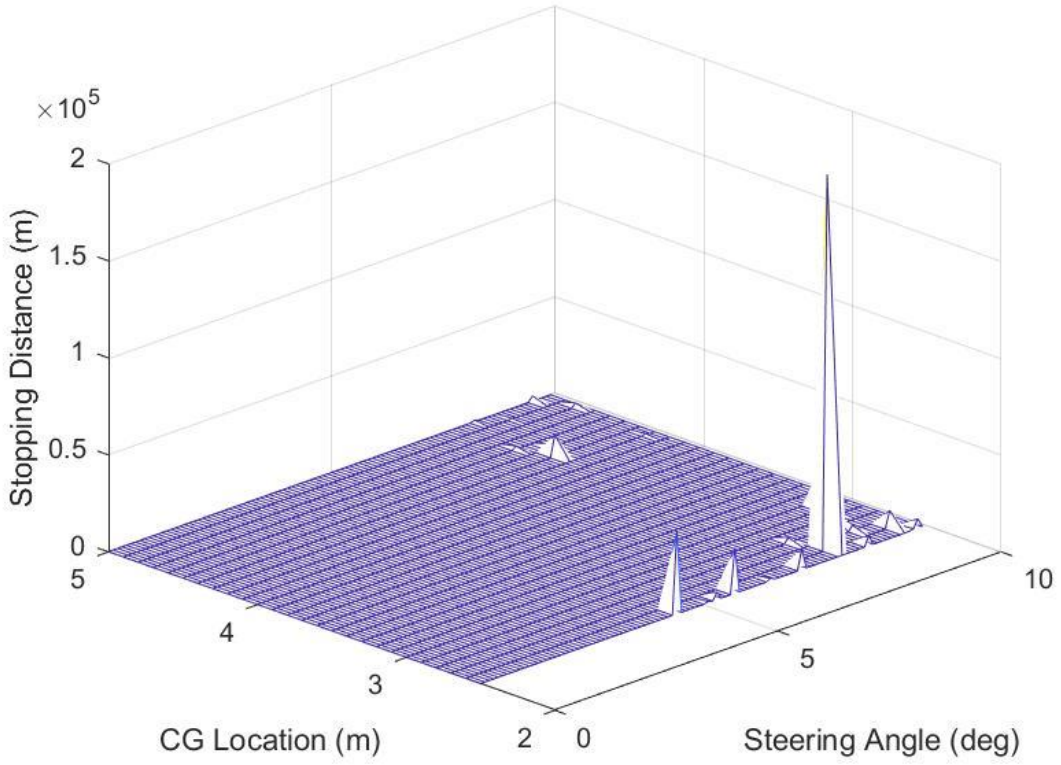

Figure 4.3: From the third run, the region of operation if further narrowed. Again there is still jackknifing events but the magnitude is reduced.

Narrowing down the region of interest again to 2.8-5m trailer CG location and the steering angle reduced to 0-7 degrees. The 3D plot is shown in Figure 4.4.

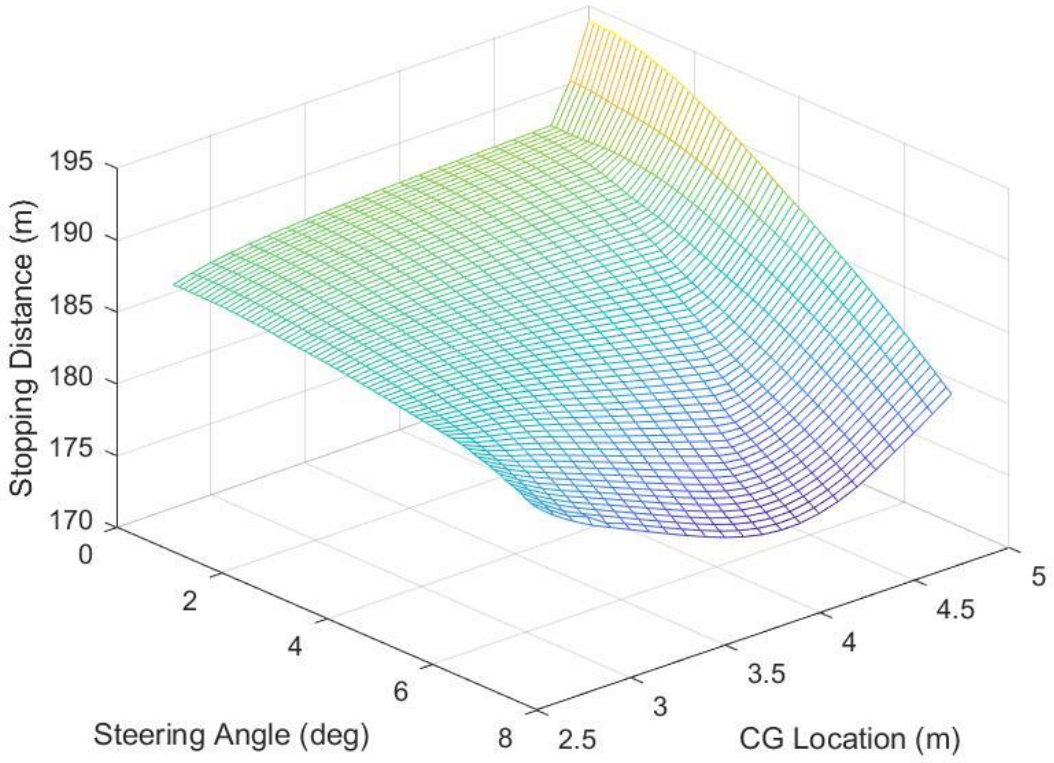

Figure 4.4: The fourth run shows the final region of operation for the tractor-trailer given the set parameters.

Figure 4.4 shows the region of operation obtained for the tractor-trailer given the selected parameter. From the figure, it can be seen how an increased steering angle and CG location reduces the stopping distance and that there are no spikes to signal jackknifing as seen in the previous figures. These are the trends that will be researched in the sections below along with determining the difference between disc and drum brakes.

After observing how the parameters of steering angle and trailer CG location, the other parameters are now varied. In Figure 4.5 through Figure 4.12 show how the varied parameters of drum and disc brakes and coefficient of friction will limit or increase the region of operation. The plots below show not only the final stopping distance, but also the maximum angle between the tractor and trailer during each steering angle and trailer CG pair. The plots covered in Figure 4.5 through Figure 4.12 are the ones highlighted in blue on Table 4.2.

The first set of results shown in Figure 4.5 and Figure 4.6 cover the first set of parameters: drum brakes, coefficient of friction of 0.8, initial velocity of 70 mph, and an 80,000 lb vehicle.

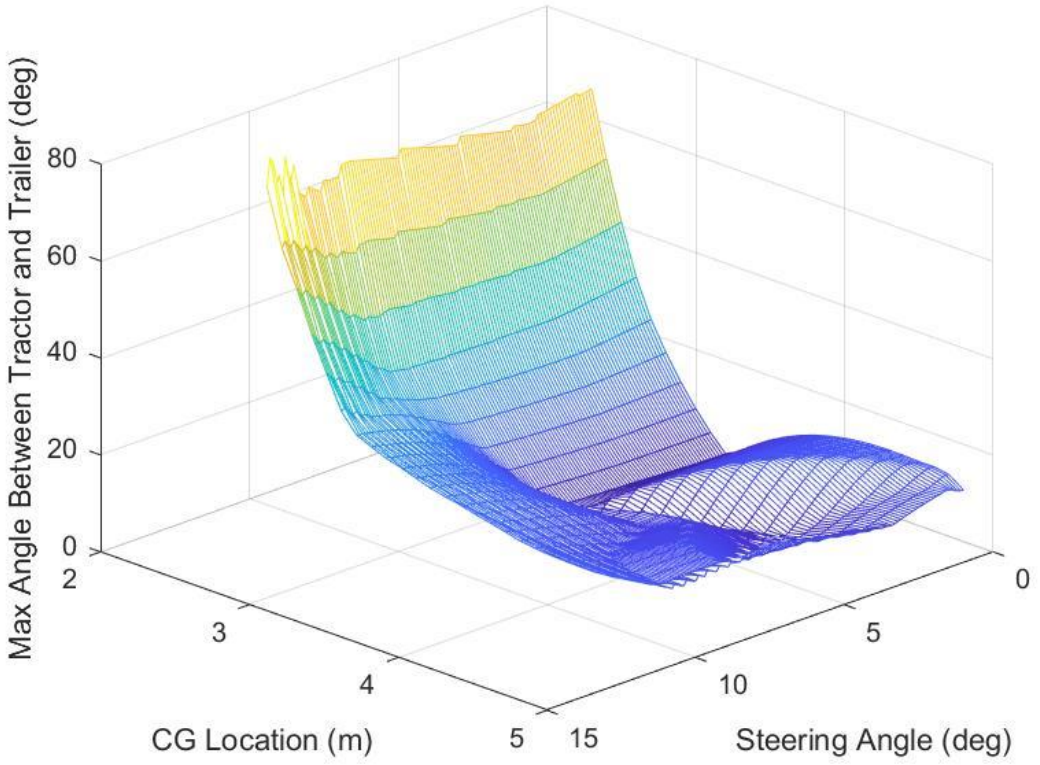

Figure 4.5: Tractor and trailer max angle during simulations using 0.8 coefficient of friction, drum brakes, 60,000 lb trailer, and initial velocity of 70mph.

It is important to keep in mind that when observing the tractor and trailer max angle plots that the plot shows only the maximum angle in that simulation. The purpose of Figure 4.5 is to show the trend that the steering angle and trailer CG location has on the maximum angle on the vehicle. From the plot, it can be seen that the closer the CG location is to the fifth wheel, the greater the maximum angle becomes and closer to jackknifing. In addition, as seen in the plot, the greater the steering angle of the tractor, the more likely maximum angle between the tractor and trailer will be larger. Figure 4.6 shows the stopping distance acquired with the same parameters as used in Figure 4.5.

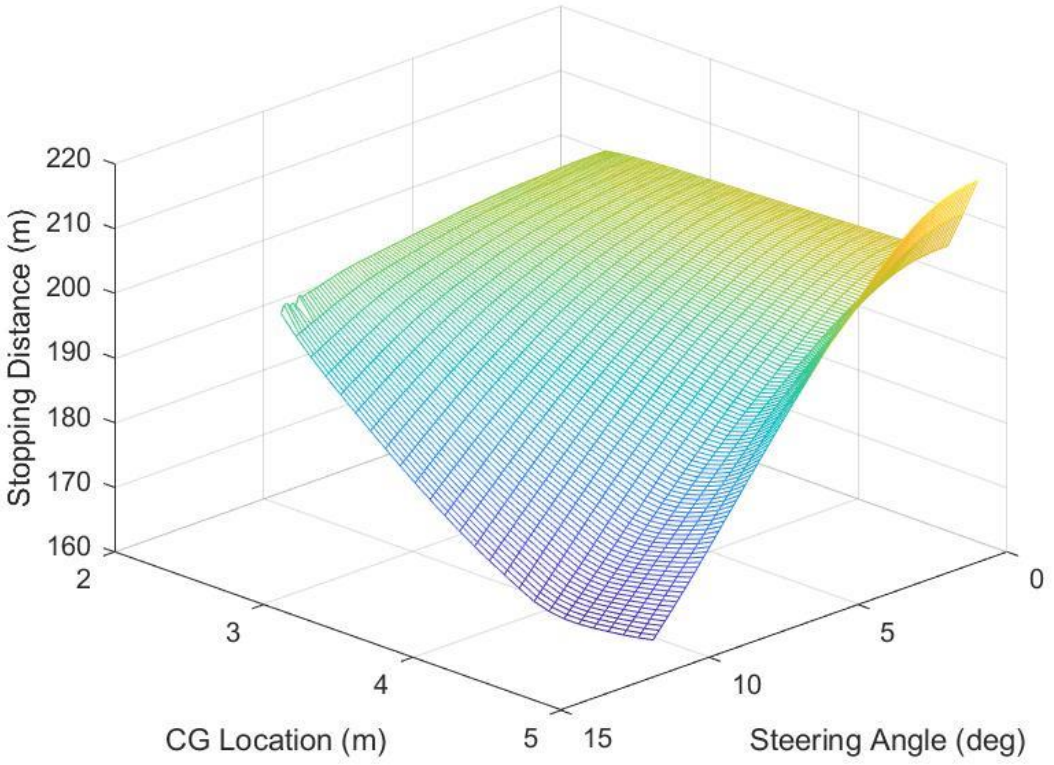

Figure 4.6: Tractor and Trailer stopping distance during simulations using 0.8 coefficient of friction, drum brakes, 60,000 lb trailer, and initial velocity of 70mph.

Looking at Figure 4.6, the effects of steering angle and trailer CG location on the stopping distance can be seen. As the steering angle and trailer CG location increase the stopping distance decrease. The stopping distance decreases from the trailer CG location moving towards the rear axle due to more weight being applied to the back wheels which allows for a greater braking force. As the steering angle increase and subsequently the trailer angle relative to the tractor as seen in Figure 4.5, so too does the cornering force which will also help the vehicle to slow down given a larger angle and also more weight on the rear axle.

In order to continue making comparisons over additional parameter changes, the next variable change to be conducted is to change the brake parameters from drum to disc while holding the other parameters the same. Figure 4.7 shows the affect that the drum brakes have on the trailer angle.

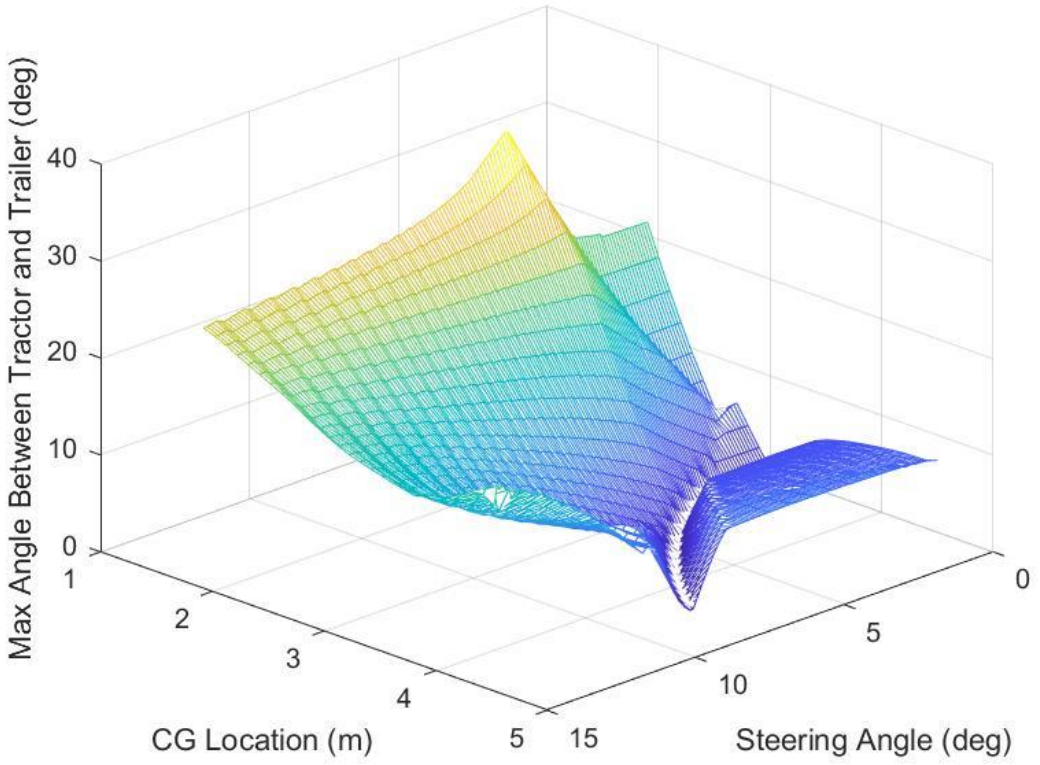

Figure 4.7: Tractor and trailer max angle during simulations using 0.8 coefficient of friction, disc brakes, 60,000 lb trailer, and initial velocity of 70mph.

Comparing Figure 4.7 to Figure 4.5, the max angle between the tractor and trailer is reduced from 80^{o} to approximately 25^{o} when looking at the largest angle in Figure 4.5. Because the tractor-trailer is much more stable with disc brakes, the tractor can have a greater steering angle as well. Next looking at Figure 4.8, the stopping distance with disc brakes can be observed.

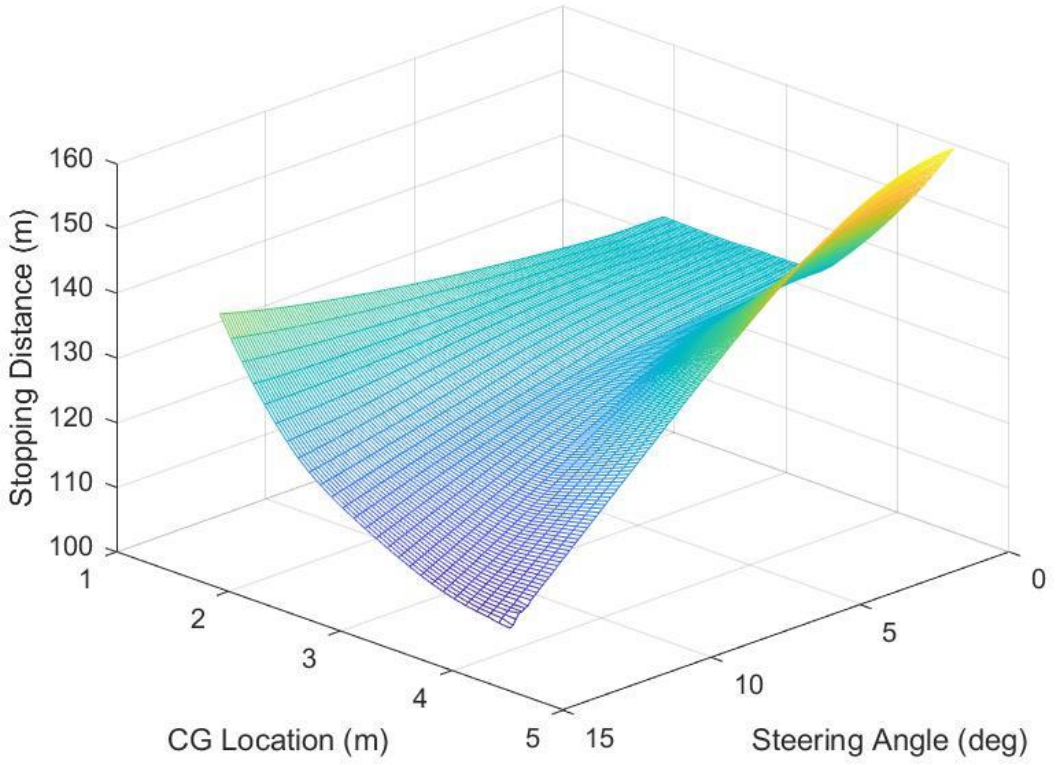

Figure 4.8: Tractor and Trailer stopping distance during simulations using 0.8 coefficient of friction, disc brakes, 60,000 lb trailer, and initial velocity of 70mph.

Looking at Figure 4.8 and Figure 4.6, the drum brakes best stopping distance was approximately 170 m compared to the disc brakes best performance at approximately 110 m. Overall, the disc brakes performed much better than the drum brakes. The disc brakes helped reduce the angle between the tractor and trailer and allow the tractor to have a greater steering angle as suggested by Dunn and Hoover [25].

After comparing drum and disc brakes, the effect of the friction shall now be simulated by changing it from the dry condition of 0.8 to a wet condition of 0.3. Figure 4.9 shows the effect of the wet conditions with drum brakes.

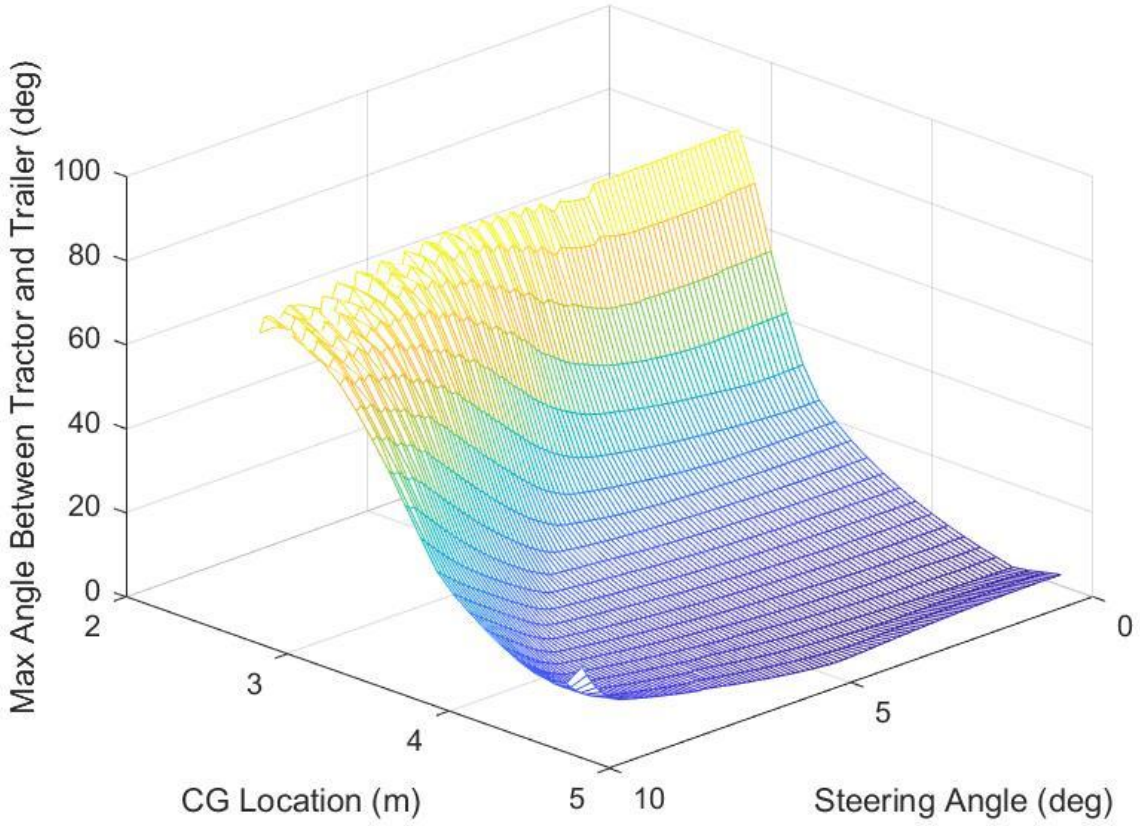

Figure 4.9: Tractor and trailer max angle during simulations using 0.3 coefficient of friction, drum brakes, 60,000 lb trailer, and initial velocity of 70mph.

While the tractor-trailer angle may seem to be more stable comparing Figure 4.9 to Figure 4.5, it is due to the reduced trailer CG location. If the simulation had the CG location the same as Figure 4.5, the user would see the jackknifing events. Next, Figure 4.10 will show the stopping distance with the wet conditions.

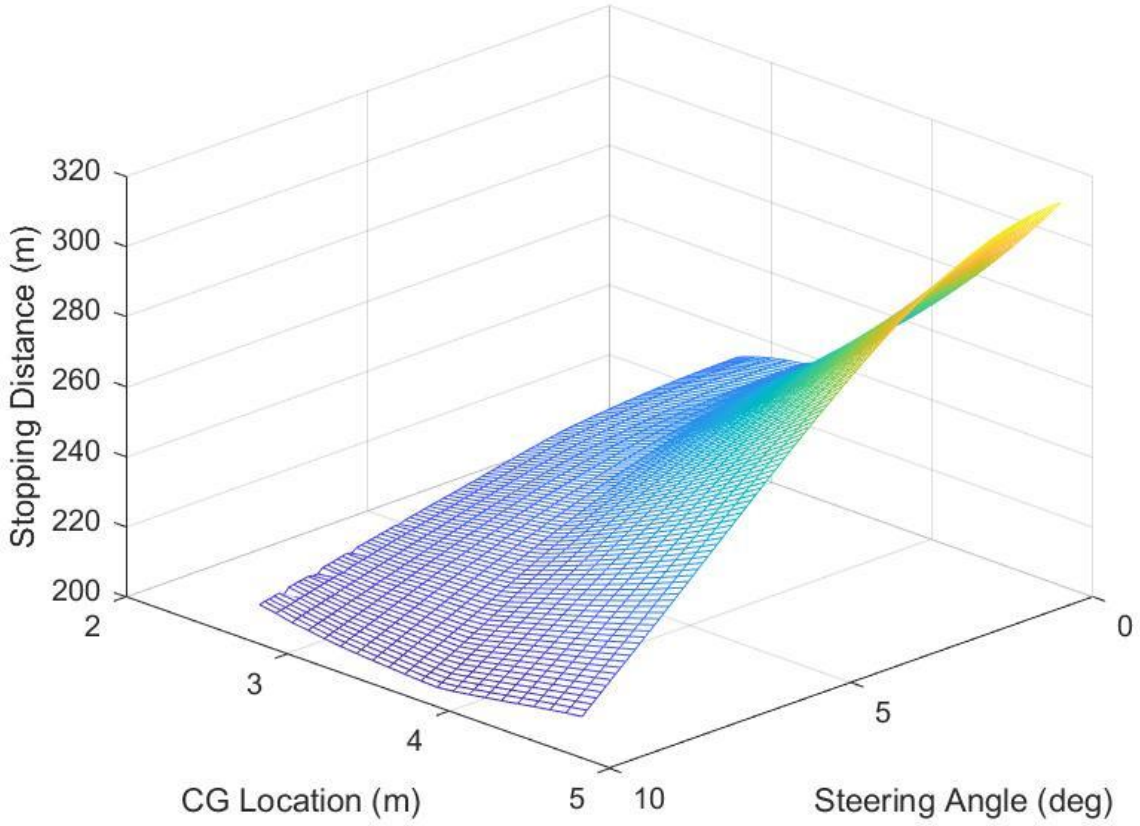

Figure 4.10: Tractor and Trailer stopping distance during simulations using 0.3 coefficient of friction, drum brakes, 60,000 lb trailer, and initial velocity of 70mph.

Looking at Figure 4.10 the effect that the wet conditions has on the stopping distance can be seen due to its increased distance compared to Figure 4.6. The vehicle under wet condition has at least a 30 m increase in the stopping distance. While it is still possible to drive on the wet roads and stop with drum brakes, it is crucial for the end user to spec out a sensor that will have the appropriate range of approximately 315 m.

Now the final comparison for this chapter shall be made by still looking at the wet road conditions, but changing the brake parameters to disc brakes. Figure 4.11 shows the max angle between the tractor and trailer with the disc brakes and wet conditions.

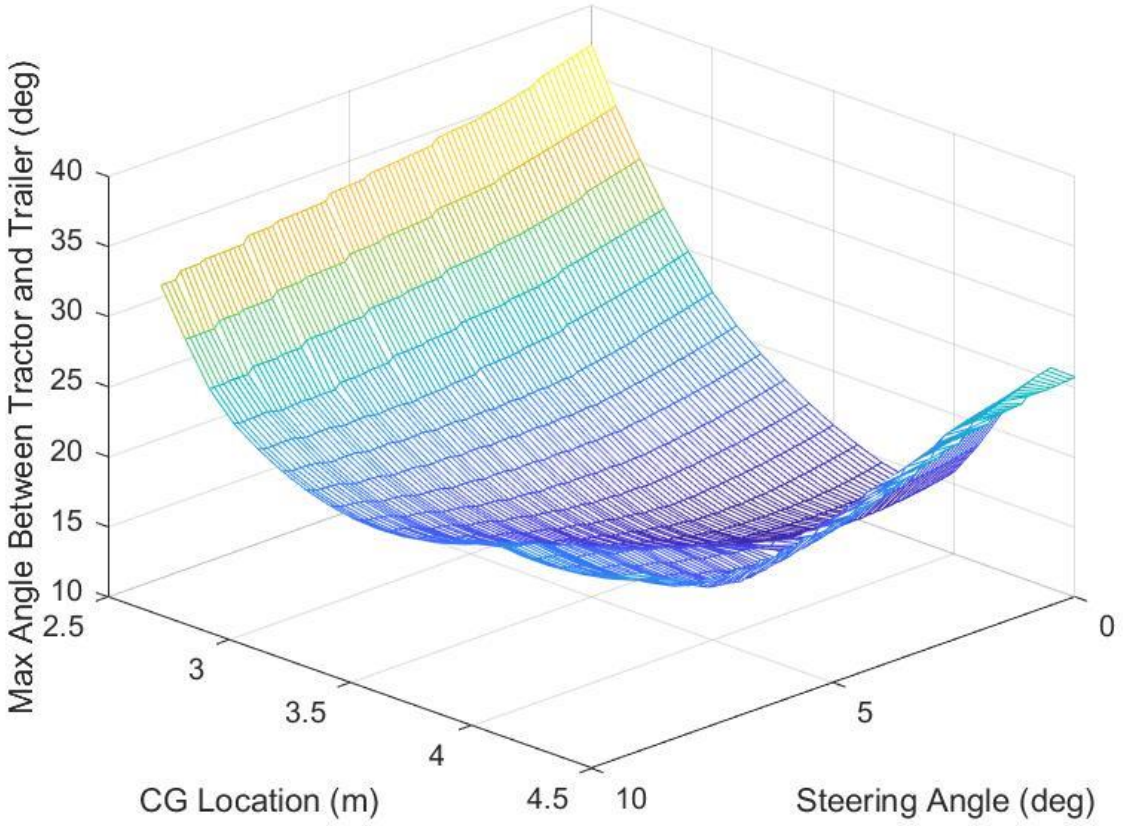

Figure 4.11: Tractor and Trailer max angle during simulations using 0.3 coefficient of friction, disc brakes, 60,000 lb trailer, and initial velocity of 70mph.

As expected when comparing Figure 4.11 to Figure 4.7 the slick conditions cause the max angle between the tractor and trailer to increase. While the plots look fairly similar, the region of operation has its trailer CG location reduced closer towards the fifth wheel. In addition to the reduced region of operation, the wet conditions also affect the stopping distance as seen in Figure 4.12.

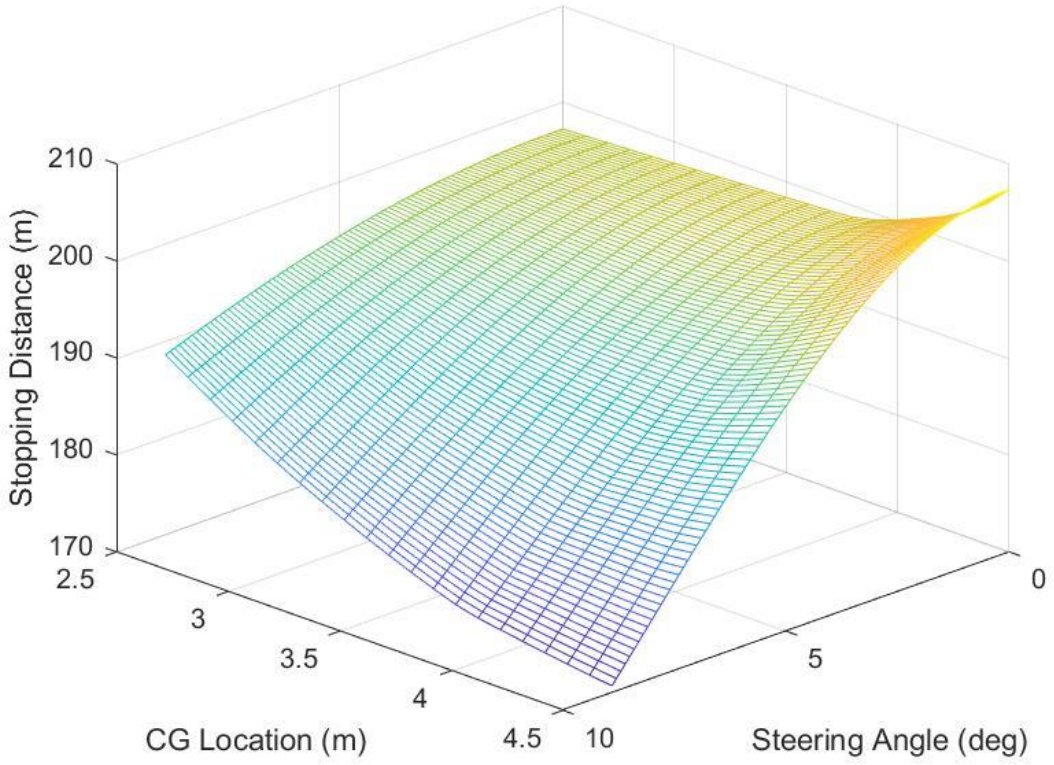

Figure 4.12: Tractor and Trailer stopping distance during simulations using 0.3 coefficient of friction, disc brakes, 60,000 lb trailer, and initial velocity of 70mph.

Similar to the drum brakes, the disc brakes have an increased stopping distance on the wet road conditions. Comparing Figure 4.12 to Figure 4.8, the wet conditions cause the vehicle to have at an average additional 60 m to stop. For a tractor-trailer with disc brakes, the max stopping distance is approximately 200 m under the conditions tested here. A range sensor, therefore, needs to have a range of the same value.

Revisiting the table of simulations, the results for each of the simulations is shown in Table 4.3. The results captured show the average, max and min stopping distance, and the max angle. Additionally, the operating range used to acquire the results is shown. This range is what was used to avoid jackknifing events under the given parameters.

Table 4.3: Summation of simulation results.

Delay (sec)	0.55															
Weight	50,000								80,000							
Brake Type	Drum				Disc				Drum				Disc			
Coefficient of Friction	0.3		0.8		0.3		0.8		0.3		0.8		0.3		0.8	
Initial Speed	60	70	60	70	60	70	60	70	60	70	60	70	60	70	60	70
Average Stopping Distance (m)	149.28	197.07	107.45	140.36	145.76	191.55	79.92	103.22	182.46	248.57	144.85	188.7	141.99	192.38	102.26	131.38
Max Stopping Distance (m)	163.87	213.25	121.31	156.46	151	198.05	86.48	111.5	242.21	315.68	173.33	202.69	154.66	209.84	126.07	159.29
Min Stopping Distance	139.3	187.04	101.34	134.47	129.89	175.59	76.27	98.93	152.96	216.62	119.9	156.16	112.29	170.43	89.18	109.49
Max Angle (deg)	65.2	62.46	46.42	52.7	65.2	69.69	29.78	32.18	85.76	88.14	53.93	62.43	50.79	62.03	29.89	39.08
Steering Angle Range (deg)	0-9	0-7	0-11	0-9	0-10	0-8	0-14	0-10	0-12	0 - 8	0-13	0-12	0-15	0 -9	0-15	0-15
Trailer CG Location (m)	2.6-5	3.1-4.9	2.2-4.9	2.3-4.8	2.6-4.5	2.9-4.3	1.5-4	1.5-4.0	2.5-5.0	2.7 - 4.9	2.3-5	2.4-4.5	2 - 4.3	2-4.6	2.0 - 4.8	1.8-4.5

The results obtained verify the decreased stopping distance and jackknifing stability that disc brakes provide compared to drum brakes. As expected from Dunn and Hoover [25] in almost every case, the disc brakes outperformed the drum brakes especially at higher weights. Looking at just these cases, the task of selecting a forward-looking perception clearly depends on road conditions and brakes used. The max stopping distance seen for the tractor-trailer was obtained under wet conditions traveling at 70 mph (315.68 m). For disc brakes, the max stopping distance

was obtained under wet conditions traveling at 70 mph (209.84 m). A forward looking sensor will, therefore, need to the same corresponding range.

While the simulations shown in this chapter are a small set of conditions that can be tested, they provide a sample for the end user to consider for a tractor-trailer. Various parameter can be changed and simulations can be explored so that operation regions and senor range requirements can be obtained.

4.3: Proposed Sensors

Now that the model has acquired a range of stopping distances to consider for a turning tractor-trailer, an appropriate selection of forward looking perception sensors can be presented for the end users consideration. Using the researched technologies from the Literature Review of, the specific sensors that have the range necessary shall be compared while also discussing some of the potential processing delays associated with the individual sensor.

The first sensors considered shall be LiDAR sensors. While looking at these sensors, it is also crucial to consider the delays associated with them for both processing and the time it takes a sensor to sweep through an area. For some of the sensors, the physical sensor will rotate about its axis to obtain a full 360^{o} range as seen with Velodyne sensors. Regardless, the sensors will sweep through an area before looking again at a point, which introduces some delay.

Using the delays for LiDAR discussed earlier, the total delay time can be determined by adding the scanning frequency to the processing delay [16]. As seen in Table 4.4, a few LiDARs were researched for their respective range, resolution, and frequency and with the researched frequency the total delay was calculated.

Table 4.4: LiDAR market research with total delay for each sensor.

Sensor	Range (m)	Resolution (cm)	Frequency (Hz)	Total Delay (sec)
Velodyne HDL-64E [8]	120	±2	5	0.2
Velodyne HDL-32E [34]	100	±2	5	0.2
Sick LD-MRS800001 [35]	300	±4	12.5	0.08
Ouster OS-$2^{(64)}$ [36]	250	±3	10	0.1

In order to appropriately recommend specific cameras for an autonomous tractor-trailer, there are several factors that must first be considered. In addition to selecting a camera, the proper lens must be chosen. A camera that has to see and identify an object must have a field of view (FOV) with the proper resolution. The factors include resolution, focal length, and sensor size. While there are many other factors that affect the image quality such as frame rate, these two factors are the qualities in a camera that will dictate whether or not an object will be identifiable

at the appropriate distance. The resolution of a camera is the dimensions in pixels that the camera will have per frame. Focal length is the distance from the lens to the camera sensor. The length dictates how large the FOV will be. The camera format is the size of the sensor in the camera that captures the image being transmitted through the lens

The horizontal width and vertical height of the scene shown in **Error! Reference source not found.** can essentially continue out any distance (*D*) given an appropriate lens and resolution. Depending on the resolution required, however, the FOV's distance, height, and width can be limited based upon how many pixels an object needs to be detected (if a focal length and camera format have already been selected). As an example if the end users desire is to identify an object 116 m away, the lens for a camera can be selected. Due to the necessity of a perception system identifying humans, an example shall be given using camera identification of a pedestrian. In order for a camera to identify a human, a box template of approximately 120 pixels height and 80 pixels width to identify a human [32]. Therefore, a cameras resolution must be approximately 65.6 pixels/m for the FOV assuming the person is roughly 1.8 m tall. Then using a calculator such as FLIR's calculator for a lens [36], the appropriate lens and focal length can be determined.

For recommendations within this thesis, Table 4.5 is presented. For this table the delay is also calculated as it was with LiDAR using the frame rate and processing time discussed [14]. Table 4.5 also contains the resolution and camera format which is needed by the end user for calculating the focal length for the end users desired range.

Table 4.5: Camera market research and total time delay.

Camera	Resolution (Pixels)	Camera Format (in)	FPS	Total Delay (sec)
Pike F-505 [41]	2452 x 2054	2/3	14	0.27
Flea3 12 MP Color USB3 Vision (Sony IMX172) [41]	4000 x 3000	1/2.3	15	0.26
Flea3 1.3 MP Color USB3 Vision (Sony IMX035) [42]	1328 x 1048	1/3	120	0.21
acA4600-10uc- Basler ace [43]	4608 x 3288	1/2.3	10	0.30
acA2040-120um – Basler ace [44]	2048 x 1536	1/1.8	120	0.21

While the cameras shown in Table 4.5 have a competitive delay to some of the LiDARs, the end user must consider the desired range as well. The further the range and lower resolution to

have a lower time delay means that the FOV will be decreased for the camera due to the focal length. Increasing the resolution to have a wider FOV due to a decreased focal length will mean an increased time delay. The end user must take these factors into consideration for the autonomous tractor-trailer. These factors, however, should not disqualify cameras due to additional capabilities over LiDAR and radar.

Radar sensors are not limited to one wave, multimodal radars can be used to sweep through multiple ranges around the radar. Having these options allows a vehicle either greater viewing angle or greater depths depending on the necessity. The radars considered are Smartmicro [37] [38] [39], TI [40], Bosch [41], and Delphi [42]. Table 4.6 show single frequency radars and multimodal frequency radars.

Table 4.6: Single frequency radar sensors capable for usage on an autonomous tractor-trailer.

Sensor	Max Range (m)	Resolution Accuracy (cm)	Sample Rate (ms)	Total Delay (sec)
Smartmicro Type 31 Antenna [39]	45	±12.4	50	0.51
Smartmicro Type 30 Antenna [38]	90	±12.4	50	0.51
Smartmicro Type 29 Antenna [37]	160	±12.4	50	0.51
Bosch: Mid-Range Radar [41]	0.37-160	±6.0	60	0.52
Bosch: Mid-Range Radar Rear [41]	0.37-80	±6.0	60	0.52
Delphi: Electronically Scanning Radar [42]	60-174	±5.0	50	0.52

While the radars appear to be the weakest of the sensors and have the greatest delay, they should still be considered for a tractor-trailer due to radar having better performance during inclement weather such as rain or snow. Again, the user must take the desired performance and requirements into consideration. Here multiple LiDAR, camera, and radar sensors have been presented for an autonomous tractor-trailer. Knowing the average speed to be traveled, the stopping distance, road conditions, and visibility requirements, an appropriate sensor can be selected weighing these requirements.

Chapter 5: Future Work and Conclusions

The work shown in this thesis is just a stepping stone for a user to create an autonomous vehicle. Using the code and simulations, a user can obtain safe regions of operation to avoid jackknifing and select a forward-looking perception sensor based upon the stopping distance. Work, however, is still required to develop the software to identify objects down the road. This is just one example of a multitude of functions required for an autonomous vehicle. The work put in is not without merit. These vehicles will assist drivers by being able to identify objects or other vehicles when humans fail to do so.

5.1: Future Work

While the information presented in this thesis covers viable sensors for perception of an autonomous tractor-trailer, there is much information and equipment that is still required before such a vehicle could ever be constructed physically and have the required software. The following list presented is a short description of several key features that need to be determined and/or created.

1. *Trailer angle detection*

Detecting the trailer angle is crucial in controlling the vehicle. Detection can potentially be done with LiDAR (through plane detection) or cameras (using region of interest and detecting differences). A motor controller unit or sensor may also be capable of determining the trailer angle relative to the tractor.

2. *Sensor suite and software for sign recognition, object detection, and lane following*

While the sensors for these requirements have been presented, the software capable for determining how the system performs these operations must be established along with additional sensors around the vehicle. This thesis has attempted to present a few ideas in the Literature Review section.

3. *Encoders for determining vehicle speed*

Vehicle control must know how fast the vehicle is going or if it is stopped. Selecting the appropriate encoders will provide feedback to the system about the current speed of the vehicle and if it is accelerating/maintaining velocity as expected.

4. *GPS*

While the vehicle may simply seem to be following lines, it is crucial that the autonomous vehicle knows where it is and where it is going. The input may be point A to point B, but the means by which a vehicle gets there is not a straight line. An autonomous tractor trailer especially needs to be careful to travel where height limitations are not too low. Additionally, the vehicle should report where it is to the user in case it breaks down.

5. *Pedal actuators*

Selection of a pedal actuator will have several requirements. The pedals cannot simply be slammed on every time. An actuator must also apply force gradually. Additionally, it must be robust enough so as not to fail over time.

6. Night and inclement weather driving

Night and inclement weather are two difficult areas for a vehicle to handle. A human driver can have difficulty enough in these conditions. In terms of night driving, radar and LiDAR will operate the same. If the vehicle is using cameras for lane and sign detection, however, operations may be interfered with. Additionally, inclement weather like snow may affect all three of these sensors types.

7. Tractor-trailer dynamics maneuvering in forward and reverse

Predicting how the tractor-trailer behaves during maneuvers will allow the autonomous vehicle to plan its own maneuvering.

8. Steering control

Keeping the steering wheel steady and moving it with the proper sensitivity will allow the autonomous vehicle to have smooth travel, turns, and lane shifts. The software and hardware for performing steering wheel movement will need to be determined.

9. Road friction

The road friction is not something that is held constant. Over the course of a single route, the road friction can change drastically. Whether the road is wet or covered in snow or simply worn down, detecting what the road condition is will enable an autonomous tractor-trailer to better anticipate how it will need to maneuver or if it needs to slow down.

10. Center of gravity of tractor and trailer

While in modeling the center of gravity may be fixed at a point, the center of gravity shifts in practical applications due to goods or components moving. In order to adequately control the vehicle especially since the loads tend to be very large and change every shipment, having a sensor that can determine where the center of gravity is will help the software better plan stopping and maneuvering.

11. Convoying

Although not absolutely crucial to creating an autonomous system, incorporating convoying between vehicles will cut on fuel costs and help prevent accidents.

While each of these tasks requires significant research and work, the groundwork for some of these areas has been created. The vehicle model created to test the stopping distance can be converted into a plant model for vehicle dynamics and controls testing. The parameters researched and the forces created in MATLAB® can all be used for further research in these areas.

5.2: Conclusion

This research paper derived a means of analyzing tractor-trailer dynamics while braking, including an indication of a jackknife condition. The results showed that under the derived set of parameters and assumptions, a forward-looking perception sensor must have a range greater than 315 m or 210 meters for a vehicle with drum or disc brakes, respectively, so that an automated system has sufficient margin to avoid obstacles in the roadway. Additionally, the research provided insight onto jackknifing events and how disc brakes (under the simulated conditions) provides greater yaw stability. The model created also provides the end user with a tool by which a wide range of parameters can be simulated.

Of the three sensor technologies researched, radar while having comparable range to the other sensors had considerable longer delay times. LiDAR showed to be the best for both range and sensor delay time. For the end user, however, driving conditions such as weather may be a greater factor when considering a sensor.

Autonomous tractor-trailers are now capable with the advancement of various perception technologies, closed loop system response, and fail-safe design. By placing these perception technologies and improved braking systems onto an autonomous tractor-trailer, the system would have sufficient range to see down the road, stop in time, and not jackknife as readily. These autonomous vehicles even if all they end up doing is assisting a driver may lead to safer driving and fewer roadway mishaps and fatalities.

Chapter 6: References

[1] NHTSA, "Critical Reasons for Crashes Investigated in the National Motor Vehicle Crash Causation Survey," February 2015. [Online]. Available: https://crashstats.nhtsa.dot.gov/Api/Public/ViewPublication/812115. [Accessed 8 November 2017].

[2] NHTSA, "2016 Fatal Motor Vehicle Crashes: Overview," October 2017. [Online]. Available: https://crashstats.nhtsa.dot.gov/Api/Public/ViewPublication/812456. [Accessed 8 November 2017].

[3] "Large Truck and Bus Crash Facts 2015," Federal Motor Carrier Safety Administration, 7 April 2017. [Online]. Available: https://www.fmcsa.dot.gov/safety/data-and-statistics/large-truck-and-bus-crash-facts-2015. [Accessed 8 November 2017].

[4] Bureau of Transportation Statistics , "National Transportation Statistics," U.S Department of Transportation.

[5] Chen et al., "Design of a Multi-Sensor Cooperation Travel Enviornment Perception System for Autonomous Vehicle," *Sensors,* vol. 12, no. 12, pp. 12386-12404, 2012.

[6] L. Zhou, Foundations and Practical Applications of Cognitive Systems and Information Processing Obstacle Detection for On-Road Vehicle Based on Range and Visual Information Fusion, Heidelberg: Springer, 2014.

[7] Chen et al., "TerraMax™: Team Oshkosh urban robot," *Journal of Field Robotics,* vol. 25, no. 10, pp. 841-860, 2008.

[8] Diamantas, Astaras, and Pnevmatikakis, "Depth Estimation in Still Images and Videos Using a Motionless Monocular Camera," *IEEE,* pp. 129-134, 2016.

[9] Ventroux, Schmit, Pasquet, Viel, and Guyetant, "Stereovision-Based 3D Obstacle Detection for Automotive Safety Driving," *IEEE,* 2009.

[10] Silvious, Wellman, Tahmoush, and Clark, "Radar System on a Large Autonomous Vehicle for Pedestrian Avoidance," *SPIE,* vol. 7669, 2010.

[11] T. Instruments, "TI Designs: TIDEP-0092," [Online]. Available: http://www.ti.com/lit/ug/tidud36a/tidud36a.pdf. [Accessed 23 October 2017].

[12] J. Lan and M. Zhang, "A New Vehicle Detection Algorithm for Real-tim Image Processing System," in *International Conference on Computer Application and System Modeling*, 2010.

[13] S. Ren, K. He, R. Girshick and J. Sun, "Faster R-Cnn: Towards Real-Time Object Detection with Region Proposal Networks," *IEEE Transactions on Pattern Analysis and Machine Intelligence,* vol. 39, no. 6, pp. 1137-1149, 2016.

[14] L. Chen, J. Yang and H. Kong, "Lidar-historgram for Fast Road and Obstacle Detection," in *IEEE International Conference on Robotics and Automation*, Singapore, 2017.

[15] J. S. Ha, G. C. Park, J. S. Lee, B. L. Cho, S. G. Sun, D. H. Kim and S. Nam, "Forward Imaging Radar Data Processing Using Scaling Factor," in *IEEE Computer Society*, 2011.

[16] NHTSA, "Federal Motor Vehicle Safety Standards; Air Brake Systems," Department of Transportation, 2009.

[17] F. P. Beer and E. R. Johnston Jr., Vector Mechanics for Engineers, R. R. Donnelley & Sons Company, 1977.

[18] Mathematics & Science Learning Center Computer Laboratory, "Numerical Methods for Solving Differential Equations The Runge-Kutta Method," San Joaquin Delta College, 2017. [Online]. Available: http://calculuslab.deltacollege.edu/ODE/7-C-3/7-C-3-h.html. [Accessed 1 January 2019].

[19] J. M. Miller, Propulsion Systems for Hybrid Vehicles, London: The Institution of Engineering and Technology, 2008.

[20] R. Limpert, Brake Design and Safety, 2011.

[21] Dunn, Heydinger, Rizzoni, and Guenther, "In-Depth Analysis of the Influence of High Torque Brakes on the Jackknife Stability of Heavy Trucks," 10-12 November 2003. [Online]. [Accessed 6 December 2017].

[22] Hoover and Dunn, "Class 8 Truck Tractor Braking Performance Improvement Study," May 2004. [Online]. Available: https://www.nhtsa.gov/sites/nhtsa.dot.gov/files/doths809700.pdf. [Accessed 14 December 2017].

[23] P. V. Dorion, "Feasibility of Anti-Jackknifing Systms for Tractor Semitrailers," *SAE International,* vol. 98, pp. 130-144, 1989.

[24] R. A. Hahn, "GPS-Based Real-Time Identification of Tire–Road Friction Coefficient," *IEEE TRANSACTIONS ON CONTROL SYSTEMS TECHNOLOGY*, pp. 331-343, May 2002.

[25] R. Wang and J. Wang, "Tire–road Friction Coefficient and Tire Cornering Stiffness Estimation Based on Longitudinal Tire Force Difference Generation," *Control Engineering Practice,* no. 21, pp. 65-75, 2012.

[26] J. Walker, "The Physics of Braking Systems," StopTech LLC, 2005.

[27] I. Schwarts, "Runge Kutta 4th Order ODE," 16 January 2013. [Online]. Available: https://www.mathworks.com/matlabcentral/fileexchange/29851-runge-kutta-4th-order-ode. [Accessed 21 December 2018].

[28] "HDL-64E," Velodyne LiDAR, [Online]. Available: http://velodynelidar.com/hdl-64e.html. [Accessed 18 October 2017].

[29] "HDL-32E," Velodyne LiDAR, [Online]. Available: http://velodynelidar.com/hdl-32e.html. [Accessed 18 October 2017].

[30] SICK AG Waldkirch, "LD-MRS 3D LiDAR Sensors," 9 June 2017. [Online]. Available: https://sick-virginia.data.continum.net/media/docs/3/03/803/Operating_instructions_LD_MRS_3D_LiDAR_sensors_en_IM0032803.PDF. [Accessed 1 February 2018].

[31] Ouster, "OS-2(64): Powered by Ouster's 5th Generation Custom Silicon," Ouster, [Online]. Available: https://www.ouster.io/product-os2/. [Accessed 3 January 2019].

[32] Collins, Gross, and Shi, "Silhouette-based Human Identification from Body Shape and Gait," *IEEE*, pp. 366-371, 2002.

[33] "Lens Calculator," FLIR Machine Vision, [Online]. Available: https://www.ptgrey.com/Lens-Calculator. [Accessed 19 October 2017].

[34] Allied Vision, "Pike F-505," [Online]. Available: file:///C:/Users/james/Downloads/Pike_DataSheet_F-505_V6.2.1_en.pdf. [Accessed 3 January 2019].

[35] Flir Machine Vision, "Flea3 12 MP Color USB3 Vision (Sony IMX172)," Flir, [Online]. Available: https://www.ptgrey.com/flea3-12-mp-color-usb3-vision-sony-imx172. [Accessed 3 January 2019].

[36] Flir Machine Vision, "Flea3 1.3 MP Color USB3 Vision (Sony IMX035)," Flir, [Online]. Available: https://www.ptgrey.com/flea3-13-mp-color-usb3-vision-sony-imx035-camera. [Accessed 3 January 2019].

[37] Basler, "acA4600-10uc-Basler ac," Basler, [Online]. Available: https://www.baslerweb.com/en/products/cameras/area-scan-cameras/ace/aca4600-10uc/. [Accessed 3 January 2019].

[38] Basler, "acA2040-120um - Basler ace," Basler, [Online]. Available: https://www.baslerweb.com/en/products/cameras/area-scan-cameras/ace/aca2040-120um/. [Accessed 3 January 2019].

[39] Smartmicro, "UMRR Automotive Type 29 Data Sheet.doc," 20 August 2014. [Online]. Available: http://www.smartmicro.de/fileadmin/user_upload/Documents/Automotive/UMRR_Automotive_Type_29_Data_Sheet.pdf. [Accessed 31 October 2017].

[40] Smartmicro, "UMRR Automotive Type 30 Data Sheet.doc," 20 August 2017. [Online]. Available: http://www.smartmicro.de/fileadmin/user_upload/Documents/Automotive/UMRR_Automotive_Type_30_Data_Sheet.pdf. [Accessed 31 October 2017].

[41] Smartmicro, "UMRR Automotive Type 31 Data Sheet.doc," 20 August 2014. [Online]. Available: http://www.smartmicro.de/fileadmin/user_upload/Documents/Automotive/UMRR_Automotive_Type_31_Data_Sheet.pdf. [Accessed 31 October 2017].

[42] T. Instruments, "TI Designs: TIDEP-0092," [Online]. Available: http://www.ti.com/lit/ug/tidud36a/tidud36a.pdf. [Accessed 31 October 2017].

[43] Bosch, "Mid-Range Radar Sensor (MRR) for Front and Rear Applications," 2015. [Online]. [Accessed 31 October 2017].

[44] Stanislas and Peynot, "Characterisation of the Delphi Electronically Scanning Radar for Robotics Applications," *Australasian Conference on Robotics and Automation, ACRA*, 2015.

[45] "Renewing Drum-brake Shoes," How a Car Works, [Online]. Available: https://www.howacarworks.com/brakes/renewing-drum-brake-shoes. [Accessed 18 October 2017].

[46] "CCTV Lens Field of View Calculator," Super Circuits, [Online]. Available: https://www.supercircuits.com/resources/tools/fov-calculator. [Accessed 19 October 2017].

[47] "Calculating Camera Sensor Resolution and Lens Focal Length," National Instruments, 13 December 2016. [Online]. Available: http://digital.ni.com/public.nsf/allkb/1BD65CB07933DE0186258087006FEBEA. [Accessed 19 October 2017].

[48] "Blackfly 5.0 MP Color GigE PoE (Sony IMX264)," FLIR Machine Vision, [Online]. Available: https://www.ptgrey.com/blackfly-50-mp-color-gige-poe-sony-imx264-2. [Accessed 19 October 2017].

[49] "Blackfly S Color 20.0 MP USB3 Vision (Sony IMX183)," FLIR Machine Vision, [Online]. Available: https://www.ptgrey.com/blackfly-s-color-200-mp-usb3-vision-sony-imx183?useripforwarding=false. [Accessed 19 October 2017].

[50] "Basler acA4600-10uc-Basler Ac," Basler, [Online]. Available: https://www.baslerweb.com/en/products/cameras/area-scan-cameras/ace/aca4600-10uc/. [Accessed 19 October 2017].

[51] T. Szakacs, "Modelling and Simulation of Tow Angle Between Agricultural Tractors and Trailers," March 2010. [Online]. Available: https://www.landtechnik-online.eu/ojs-2.4.5/index.php/landtechnik/article/download/2010-3-178-181/731. [Accessed 26 November 2017].

[52] T. Efficiency, "5th Wheel Settings," [Online]. Available: http://www.truckingefficiency.org/tractor-aerodynamics/5th-wheel-settings. [Accessed 27 November 2017].

[53] Maddern, Pascoe, Linegar, and Newman, "1 Year, 1000km: The Oxford RobotCar Dataset," *International Journal of Robotics Research*, vol. 36, no. 1, pp. 3-15, 2017.

[54] M. B. Lascurain, "Effects of Tire Rolling Resistance on Class 8 Tractor-Trailer Stopping Distance," National Highway Traffic Safety Administration, Washington DC, 2015.

[55] SAE International, "Levels of Driving Automation are Defined in New SAE Internation Standard J3016," 2014. [Online]. Available: https://www.sae.org/misc/pdfs/automated_driving.pdf. [Accessed 8 November 2017].

[56] Ball, Danaher, and Buss, "Full-Scale Testing and Analysis of Tractor-Trailer," SAE International, 2010.

[57] Garrott, Heitz, and Bean, "Experimental Measurement of the Stopping Performance of a Tractor-Semitrailer From Multiple Speeds," National Highway Traffic Safety Administration, Washington DC, 2011.

[58] U.S. Department of Transportation Federal Highway Administration, "Federal Size Regulations for Commercial Motor Vehicles," October 2004. [Online]. Available: https://ops.fhwa.dot.gov/freight/publications/size_regs_final_rpt/. [Accessed 26 November 2017].

[59] Alexander, Donath, Hennessey, Morellas, Shankwitz, "A Lateral Dynamic Model of a Tractor-Trailer: Experimental Validation," November 1996. [Online]. Available: http://dotapp7.dot.state.mn.us/research/pdf/199718.pdf. [Accessed 26 November 2017].

Chapter 7: Appendix A

Appendix A contains the code used to generate the simulations. Greater definition of each section can be found in Chapter 3.

```
%% Simulation of Tractor-Trailer Braking During Turning
% The purpose of this simulation is to provide the end user with a
% parameterizable simulation of a tractor-trailer braking and coming to a
% complete stop during a turn. This program will provide the end user with
% conditions with which jackkniffing will occur and regions with which
% the tractor-trailer may operate safely.

%Author: James Nathan Quartuccio

%Clearing the workspace, command window, and closing windows
clc
clear
close all


%Initalizing the tractor, trailer, and other variables
h1 = 1.4;       %height from the bottom of the wheel to the tractor cg (m)
h2 = 1.5;       %height from the bottom of the wheel to the trailer cg (m)
h3 = .5;        %height from the fifth wheel to the tractor cg (m)
h4 = .8;        %height from the fifth wheel to the trailer cg (m)
I1 = 400000;    %moment of inertia of the tractor kg*m^2
I2 = 767667;    %moment of inertia of the trailer kg*m^2
g = 9.81;       %gravity constant m/s^2
W1 = 20000*4.448;   %weight of the tractor (N)
W2 = 30000*4.448;  %weight of the trailer (N)
m1 = W1/g;          %determining the mass of the tractor (kg)
m2 = W2/g;          %determining the mass of the trailer (kg)
ww = 2.6/2;         %distance from the axle to the wheel (m)

%Braking Parameters
R = 21*.0254;       %Wheel radius (m)
roeL = 90*6894.76;  %Brake line pressure (N/m^2)
roeo = 5*6894.76;   %Pushout pressure (N/m^2)
% roe = 5.5;          %Lever ratio for drum brakes
Ac = 30*.00064516;  %Brake chamber area (m^2)
roe = 11;           %Lever ratio for disc brakes
BF = 1.3;           %Brake factor
mum = .7;           %Mechanical efficiency
fa = .9;            %brake adjustment reduction factor
fF = .9;            %brake temperature fade reduction factor
r = 8*.0254;        %drum rotor radius (m)
```

```
%Cornering, rolling, and drag force constants
Cf = 8000;          %Cornering force coefficient
u = .3;             %Coefficient of friction for tire and road
crr = .01;          %Coefficient for rolling friction
cd = 0.654;         %Coefficient of drag
Af = 66.5*0.092903; %Frontal area of tractor (m^2)


%Tractor parameters
L1 = 2.59;              %Distance from front axle to the cg
L6 = 3.36;              %Distance from fifth wheel to the cg
L23 = 2.7+(4.02-2.7)/2; %Distance from the rear axle to the cg

%Initailizing the Hitch, Brake, and Cronering forces.
FHX(1) = 0;
FHY(1) = 0;
FHZ(1) = 0;
FB1(1) = 0;
FB23(1) = 0;
FB451(1) = 0;
FB452(1) = 0;
FC1(1) = 0;
FC23(1) = 0;
FC451(1) = 0;
FC452(1) = 0;

degrad = pi/180; %conversion from degrees to radians
raddeg = 180/pi; %conversion from radians to degrees



%Setting the time step, software processing delay, and the "b" storage variable
dt = .05;
% delay = 0; %No delay for validation to lit review documents
delay = 0.55; %Processing Delay
b = 1;


%The first for loop steps through different steering angles "stang1". The
%steering angle steps from 0.0001 deg to the desired final angle.


for alpha1 = .0001*degrad:.1*degrad:10*degrad


    %Setting the storage variables "a" and "n" to one for each loop
    a = 1;
    n = 1;
    %For each steering angle the trailer cg location (tcg) is moved as
    %desired be the user. The trailer cg location is shifted by 0.1m for
```

```
%each loop.
for tcg = 2.6:.1:4.6
   %After each loop the variables again need to be cleard so that the
   %proper values are calculated and stored
   clearvars v s vangle1 vangle2 sangle1 sang2 ...
      time ay1 ay2 ax1 ax2 AngDiff

   %Declairing the variables for the trailer cg location between the
   %fifth wheel and rear axle.
   L7 = tcg;        %Distance from the hitch to the cg
   L45 = 5.2450-tcg; %Distance from the trailer axle to the cg

   %Determinig the turning radius for the tractor (r1) and trailer
   %(r2)
   r2 = (L23+L1)/(tan(alpha1))+(ww); %turning radius of the trailer m
   r1 = sqrt((power(r2,2)+power(L23,2))); %turning radius of the tractor m


   %Setting up the initial values that will need to be cleared after
   %each simulation.
   FN1(1) = m1*g*L6/(L1+L6);
   FN45(1) = m2*g*L45/(L45+tcg);
   FN451(1) = FN45(1)/2;
   FN452(1) = FN45(1)/2;
   FN23(1) = -FN1(1)-FN45(1)+m1*g+m2*g;
   FNL(1) = FN23(1)/2+FN1(1)/2;
   FNR(1) = FN23(1)/2+FN1(1)/2;
   v(1) =  60*0.44704; %initializing velocity m/s
   th1(1) = 0;        %initializing tractor yaw acceleration rad/s^2
   th2(1) = 0;        %initializing trailer yaw acceleration rad/s^2
   vangle2(1)=0;      %initializing tractor yaw velocity rad/s^2
   vangle1(1)=0;      %initializing trailer yaw velocity rad/s^2
   s(1) = 0;          %initializing the position to zero m
   ax1(1) = 0;        %initializing the tangental acceleration of the tractor m/s^2
   ax2(1) = 0;        %initializing the tangental acceleration of the trailer m/s^2
   ay1(1)=power(v(1),2)/r1; %initializing the centripital acceleration of the tractor m/s^2
   ay2(1)=power(v(1),2)/r2; %initializing the centripital acceleration of the trailer m/s^2
   sangle1(1)= 0;     %initializing the tractor angle to zero rad
   sang2(1)=asin((L7+L45)/(power(r2,2))); %initializing the trailer
                  %angle relative to the tractor given steering
                  %angle, fifth wheel position, and cg positions
   FC1(1) = 2*u*FN1(1)*(((Cf*tan(sangle1(1)))/(u*FN1(1)))-(1/3)...
         *power(((Cf*tan(sangle1(1)))/(u*FN1(1))),2)+(1/27)...
         *power(((Cf*tan(sangle1(1)))/(u*FN1(1))),3));
   FC23(1) = 2*u*FN23(1)*(((Cf*tan(sangle1(1)))/(u*FN23(1)))-(1/3)...
         *power(((Cf*tan(sangle1(1)))/(u*FN23(1))),2)+(1/27)...
         *power(((Cf*tan(sangle1(1)))/(u*FN23(1))),3));
   FC451(1) = 2*u*FN451(1)*(((Cf*tan(sang2(1)))/(u*FN451(1)))-(1/3)...
         *power(((Cf*tan(sang2(1)))/(u*FN451(1))),2)+(1/27)...
         *power(((Cf*tan(sang2(1)))/(u*FN451(1))),3));
   FC452(1) = 2*u*FN452(1)*(((Cf*tan(sang2(1)))/(u*FN452(1)))-(1/3)...
```

```
            *power(((Cf*tan(sang2(1)))/(u*FN452(1))),2)+(1/27)...
            *power(((Cf*tan(sang2(1)))/(u*FN452(1))),3));


        %Declaing the storage vairable n and time variable for each run
        %through the for loop
        n = 1;
        time(1) = 0;

        %The last for loop is the simulation of the tractor-trailer
        %traveling from the initial velocity to zero. The loop is set up to
        %step through the desired time step until the velocity reaches
        %zero.
         for t=0:dt:600
           %The if statement is established to break the simulation when
           %the velocity of the tractor-trailer reaches zero
            if v(n)>0

              %Determing the angular velocity for each time step
              w1 (n) = v(n)/r1; %angular velocity of the tractor (rad/s)
              w2 (n) = v(n)/r2; %angular velocity of the trailer (rad/s)
%               ay1(n) = power(v(n),2)/r1;
%               ay2(n) = power(v(n),2)/r2;

              Fdrag(n) = .5*cd*Af*power(v(n),2);
              Frr1(n) = crr*FN1(n);
              Frr23(n) = crr*FN23(n);
              Frr451(n) = crr*FN451(n);
              Frr452(n) = crr*FN452(n);
              FrrL(n) = crr*FNL(n);
              FrrR(n) = crr*FNR(n);

             %Here the matricies A and B are set up to solve for x in the
             %Ax=B using Matlab's linear solver (linsolve). The x being
             %solved for are the unknown normal forces, hitch forces, and
             %tangental accelerations. The A matrix contains the constants
             %being multiplied to the x variables. The B matrix has the
             %known constants.

             %Setting up varaiables for the A matrix
              c1 = (h2-h4)*cos(sang2(n));
              c2 = (h2-h4)*sin(sang2(n));
              c3 = cos(sang2(n));
              c4 = sin(sang2(n));

             %Setting up the A matrix. The comments at the top show which
             %collums represent which unknown variables.

             A0 =[1,1,-1,0,0,0,0,0,0,0,0;... %sum z2
                 0,0,(L7+L45),-c1,c2,0,0,0,m2*h2,0,0;... %My 451
                 0,-2*ww,ww,c2,c1,0,0,0,0,0,0;...  %Mx 451
```

```
            0,0,1,0,0,1,1,0,0,0,0;... %sum z1
            0,0,0,(h1-h3),0,(L1+L23),0,m1*h1,0,0,0;... %My 231
            0,0,0,0,1,0,0,0,0,0,0;...%sum y1
            0,0,0,c3,-c4,0,0,0,m2,0,0;... %Sum x2
            0,0,0,-1,0,0,0,m1,0,0,0;... %Sum x1
            0,0,0,0,0,0,0,1,-1/c3,0,0;...   %ax1 and ax2 relationship
            0,0,-ww,0,-h1+h3,0,0,0,0,-2*ww,0;...
            0,0,1,0,0,0,0,0,0,1,1];

        %Establishing the B matrix with the known variables.
        B0 = [m2*g;...                  %Sum z2
            -m2*g*L45;...               %My 451
            m2*ay2(n)*(h2-h4)-m2*g*ww;...  %Mx 451
            m1*g;...                    %Sum z1
            m1*g*L23;...                %My 231
            FC1(n)+FC23(n)-m1*ay1(n);...   %Sum y1
            -FB451(n)-FB452(n)-Frr451(n)-Frr452(n);...        %Sum x2
            -FB1(n)-FB23(n)-Fdrag(n)-Frr1(n)-Frr23(n);...    %Sum x1
            th2(n)*L45+power(w2(n),2)*L45-th1(n)*L23-power(w1(n),2)*L23;... %ax1 and ax2
relationship
            -m1*g*ww+m1*ay1(n)*h1;...
            m1*g];

        %Using linsolve, the x variables are being solved for in
        %A^-1*A*x=A^-1*B
        F0 = linsolve(A0,B0);

        %From F0, the individual variables can be pulled.
        FN451(n+1) = F0(1,1);    %Wheel 451 Normal Force (N)
        FN452(n+1) = F0(2,1);    %Wheel 452 Normal Force (N)
        FHZ(n) = F0(3,1);      %Hitch force in the z direction (N)
        FHX(n) = F0(4,1);      %Hitch force in the x direction (N)
        FHY(n) = F0(5,1);      %Hitch force in the y direction (N)
        FN1(n+1) = F0(6,1);      %Tractor Front Normal Force (N)
        FN23(n+1) = F0(7,1);     %Tractor Rear Normal Force (N)
        ax1(n+1)=F0(8,1);      %Tractor tangental acceleration (m/s^2)
        ax2(n+1)=F0(9,1);      %Trailer tangental acceleration (m/s^2)
        FNR(n+1) = F0(10,1);
        FNL(n+1) = F0(11,1);

          %Cornering Force Calculations for the tractor
          if sangle1(n)== 0 %Setting the corning force to zero  when the angle is zero
             FC1(n+1) = 0;
             FC23(n+1) = 0;
          %calculating the corning force for the tractor angles other than zero.
          else
             FC1(n+1) = 2*u*FN1(n)*(((Cf*tan(sangle1(n)))/(u*FN1(n)))-(1/3)...
                 *power(((Cf*tan(sangle1(n)))/(u*FN1(n))),2)...
                 +(1/27)*power(((Cf*tan(sangle1(n)))/(u*FN1(n))),3));

             FC23(n+1) = 2*u*FN23(n)*(((Cf*tan(sangle1(n)))/(u*FN23(n)))-(1/3)...
```

```
        *power(((Cf*tan(sangle1(n)))/(u*FN23(n))),2)...
        +(1/27)*power(((Cf*tan(sangle1(n)))/(u*FN23(n))),3));
end

%Cornering Force Calculations for the trailer
if sang2(n) == 0 %Setting the corning force to zero  when the angle is zero
   FC451(n+1) = 0;
   FC452(n+1) = 0;
%calculating the corning force for the trailer angles other than zero.
else
   FC451(n+1) = 2*u*FN451(n)*(((Cf*tan(sang2(n)))/(u*FN451(n)))-(1/3)...
       *power(((Cf*tan(sang2(n)))/(u*FN451(n))),2)...
       +(1/27)*power(((Cf*tan(sang2(n)))/(u*FN451(n))),3));

   FC452(n+1) = 2*u*FN452(n)*(((Cf*tan(sang2(n)))/(u*FN452(n)))-(1/3)...
       *power(((Cf*tan(sang2(n)))/(u*FN452(n))),2)...
       +(1/27)*power(((Cf*tan(sang2(n)))/(u*FN452(n))),3));
end

%Calculating the braking force. The braking force starts at
%0.5 seconds due to the brake line pressure requiring build
%up pressure.
if t >= .5+delay
   FB1(n+1) = (2/(R))*((roeL-roeo)*(Ac*BF*mum*roe*fa*fF*r));
   FB23(n+1) = (2/(R))*((roeL-roeo)*(Ac*BF*mum*roe*fa*fF*r));
   FB451(n+1) = (1/(R))*((roeL-roeo)*(Ac*BF*mum*roe*fa*fF*r));
   FB452(n+1) = (1/(R))*((roeL-roeo)*(Ac*BF*mum*roe*fa*fF*r));
   FBR(n+1) = (2/(R))*((roeL-roeo)*(Ac*BF*mum*roe*fa*fF*r));
   FBL(n+1) = (2/(R))*((roeL-roeo)*(Ac*BF*mum*roe*fa*fF*r));
else
   FB1(n+1) = 0;
   FB23(n+1) = 0;
   FB451(n+1) = 0;
   FB452(n+1) = 0;
   FBR(n+1) = 0;
   FBL(n+1) = 0;
end


%Perfomring a check on the braking force. The braking force
%cannot exceed the normal force multiplied by the
%coefficient of friction.

%Checking the brake force at the front tractor axle
if FB1(n+1) > u*FN1(n)
      FB1(n+1) = u*FN1(n);
end
%Checking the brake force at the rear tractor axle
if FB23(n+1) > u*FN23(n)
      FB23(n+1) = u*FN23(n);
end
```

```
        %Checking the brake force at the trailer axle
        if FB451(n+1) > u*(FN451(n))
            FB451(n+1) = u*(FN451(n));
        end
        if FB452(n+1) > u*(FN452(n))
            FB452(n+1) = u*(FN452(n));
        end

        if FBR(n+1) > u*FNR(n)
            FBR(n+1) = u*FNR(n);
        end

        if FBL(n+1) > u*FNL(n)
            FBL(n+1) = u*FNL(n);
        end


        %Solving the final unknowns for the tractor and trailer
        %centripital acceleration and yaw acceleration.
        ay2(n+1) = (-FC451(n+1)-FC452(n+1)-cos(sang2(n))*FHY(n)...
           -sin(sang2(n))*FHX(n))/m2;
        th2(n+1) = (FC451(n+1)*L45+FC452(n+1)*L45-cos(sang2(n))...
           *FHY(n)*L7-sin(sang2(n))*FHX(n)*L7-FB452(n+1)*ww...
           +FB451(n+1)*ww-Frr452(n)*ww+Frr451(n)*ww)/I2;
        ay1(n+1) = (-FC1(n+1)-FC23(n+1)+FHY(n))/m1;
        th1(n+1) = (-FC1(n+1)*L1+FC23(n+1)*L23-FHY(n)*L6...
           +FBR(n+1)*ww-FBL(n+1)*ww-FrrL(n)*ww+FrrR(n)*ww)/I1;

        %Storing the time
        time(n+1)=t;

        %Using the runge-kutta method to integrate the acceleration
        %to acquire the next velocity value and to integrate the
        %velocity to acquire the next position value.
        v(n+1) = integrator(ax1(n),v(n),dt);
        s(n+1) = integrator(v(n),s(n),dt);
        vangle1(n+1) = integrator(th1(n),vangle1(n),dt);
        sangle1(n+1) = integrator(vangle1(n),sangle1(n),dt);
        vangle2(n+1) = integrator(th2(n),vangle2(n),dt);
        sang2(n+1) = integrator(vangle2(n),sang2(n),dt);

        n=n+1;
    end
end

%Storing the runs for plotting
Delta (a) = tcg;        %Storing the steering angle
srungeA (a) = s(end); %Storing the distance taken to stop
SA1(a) = sangle1(n);       %Storing the angle of the tractor
SA2(a) = sang2(n);       %Storing the angle of the trailer
```

```
        %Within this for loop, the program compares the angle of the
        %tractor to the trailer to determine the difference at each time
        %step
        for x = 1:1:n
            AngDiff(x) = abs(abs(sangle1(x))-abs(sang2(x)));
%             if AngDiff(x)> 45*drad
%               AngDiff(x) = 45*drad;
%             end
        end

        %After performing the comparison, the program determines what the
        %largest difference was using the "max" function
        AngDiffMax(a) = max(AngDiff);
        va2(a) = max(vangle2);

        %Changing the a value for the next set of iterations for the
        %changing trailer cg location
        a = a+1;
    end

    %Outside of the for loop for the changing trailer cg location, the
    %values obtained for the steering angle, stopping distance, tractor
    %angle, trailer angle, the angle difference between the tractor and
    %trailer are stored in the vector or cells below.

    angle(b) = alpha1;      %Storing the steering angle
    distance{b} = srungeA;  %Storing the stopping distance
    Ang1 {b} = SA1;         %Storing the tractor angle
    Ang2 {b} = SA2;         %Storing the trailer angle
    AngD {b} = AngDiffMax;  %Storing the maximum angle difference between the tractor and trailer
    VA2 {b} = va2;          %Storing the trailer angular velocity
    cg {b} = Delta;         %Storing the cg position

    %Stepping the storage variable
    b = b+1;
end


%converting the cells to be plotted
dis = reshape(cell2mat(distance),[],length(distance));
cgdis = reshape(cell2mat(cg),[],length(cg));
A2 = reshape(cell2mat(Ang2),[],length(Ang2));
A1 = reshape(cell2mat(Ang1),[],length(Ang1));
AD = reshape(cell2mat(AngD),[],length(AngD));
VA2 = reshape(cell2mat(VA2),[],length(VA2));

figure
mesh(angle*raddeg,cgdis,dis)
hold on
az = 135;
```

```
el = 30;
view(az, el);
xlabel ('Steering Angle (deg)')
ylabel('CG Location (m)')
zlabel('Stopping Distance (m)')
hold off
DisAvgM = mean(mean(dis))
% DisAvgF = mean(mean(dis))*3.28084
MaxM = max(max(dis))
MinM = min(min(dis))

figure
mesh(angle*raddeg,cgdis,AD*raddeg)
hold on
az = 135;
el = 30;
view(az, el);
xlabel ('Steering Angle (deg)')
ylabel('CG Location (m)')
zlabel('Max Angle Between Tractor and Trailer (deg)')
hold off
MaxA = max(max(AD*raddeg))
```